Fundamental physics measurements with Galileo FOC satellites and the Galileo for science project. I. A 3D-CAD and a box wing for modeling the effects of nonconservative forces

David Lucchesi,[1,2,3,*] Massimo Visco,[1,2] Carlo Lefevre,[1] Marco Lucente,[1] Francesco Santoli,[1] Feliciana Sapio,[1,4] Marco Cinelli,[1] Alessandro Di Marco,[1] Emiliano Fiorenza,[1] Pasqualino Loffredo,[1] Carmelo Magnafico,[1] Roberto Peron,[1] and Francesco Vespe[5]

[1]*Istituto Nazionale di Astrofisica (INAF), Istituto di Astrofisica e Planetologia Spaziali (IAPS), Via del Fosso del Cavaliere, 100, 00133 Roma, Italy*

[2]*Istituto Nazionale di Fisica Nucleare (INFN), Sezione di Tor Vergata, Via della Ricerca Scientifica 1, 00133 Roma, Italy*

[3]*Istituto di Scienza e Tecnologie della Informazione (ISTI), Consiglio Nazionale delle Ricerche (CNR), Via G. Moruzzi 1, 56124 Pisa, Italy*

[4]*Dipartimento di Fisica, Sapienza Università di Roma, Piazzale Aldo Moro 5, 00185 Roma, Italy*

[5]*Agenzia Spaziale Italiana (ASI), Centro di Geodesia Spaziale (CGS), Contrada Terlecchia, 75100 Matera, Italy*

(Received 16 July 2023; accepted 9 January 2024; published 12 March 2024)

This paper introduces the main problems related to the modeling of the effects of nongravitational perturbations on satellites of the Galileo FOC constellation. The problem is addressed from the point of view of the scientific objectives of the Galileo for Science (G4S_2.0) project. These objectives are reflected in a set of fundamental physics measurements that will exploit the orbits and atomic clocks aboard the Galileo satellites, in particular the GSAT-0201 and GSAT-0202 satellites characterized by elliptical orbits, and not by almost circular orbits such as in the case of the remaining satellites of the constellation. The main focus is on the modeling of the direct solar radiation pressure, the largest nongravitational perturbation on GNSS satellites. After an in-depth presentation of the main nongravitational perturbations of interest, and of the models currently in use in the literature for their consideration, the work focuses on the amplitudes of the different effects and, with particular attention, on their intrinsic knowledge. Finally, two different models are introduced for the structure of the Galileo satellite specially developed for the objectives of G4S_2.0. The first is a simple model of the box-wing type, developed on the basis of the information currently available on the characteristics of the satellite. The second is a 3D model of the Galileo spacecraft, somewhat sophisticated due to the richness of the details on the structure and the various elements that make up the surfaces of the satellite. The activities carried out and in progress with these models and those planned with their subsequent updated versions are described.

DOI: 10.1103/PhysRevD.109.062004

I. INTRODUCTION

The Galileo for Science (G4S_2.0) project [1–6], funded by the Italian Space Agency (ASI), aims to perform a set of gravitational measurements mainly using the two Galileo satellites GSAT-0201 and GSAT-0202 exploiting the relatively high eccentricity ($\simeq 0.16$) of their orbits with respect to that (≈ 0) of the other satellites of the full operational capability (FOC) constellation. These two satellites have been already considered in 2018 by both ZARM [7] and SYRTE [8] for a new measurement of the gravitational redshift that has improved the 1976 measurement of Gravity Probe A (GPA) [9,10] by a factor between 4 and 6 respectively, see also [11,12] for more recent results. In fact, from an accurate analysis of the orbits and clocks of these two Galileo satellites, a set of relativistic tests can be performed with the objectives of comparing the predictions of Einstein's theory of general relativity [13] with those of other gravitational theories [14] concerning, mainly, the motion of a "test" particle along a geodesic of space-time and the time dilation of the on-board clocks.

G4S_2.0 has four main objectives in fundamental physics plus three other main objectives that are mainly linked, but not only in truth, to technical aspects of the Galileo FOC constellation and of Global Navigation Satellite System (GNSS) satellites in general. The objectives in the field of fundamental physics are: (i) providing a new measurement of gravitational redshift; (ii) measuring

*david.lucchesi@inaf.it

the relativistic precessions of the orbits of the two satellites GSAT-0201 and GSAT-0202; (iii) placing constraints on the possible presence of dark matter in our Galaxy; (iv) providing the detection of gravitational waves. The last two objectives involve the use of the entire constellation of the Galileo FOC satellites. The other three objectives are: (v) realize a relativistic positioning system; (vi) developing new models for nongravitational forces; and (vii) realizing a new accelerometer concept for a next generation of Galileo satellites.

Three Italian research institutes are involved in G4S_2.0: Center for Space Geodesy (ASI-CGS) in Matera, Istituto di Astrofisica e Planetologia Spaziali (IAPS-INAF) in Roma and Politecnico (POLITO) in Torino.

In this work we will focus on point (vi) above and, in particular, on the direct solar radiation pressure (SRP), the largest nongravitational perturbation (NGP) on the orbit of Galileo FOC satellites and in general of all satellites of the GNSS. Indeed, the nonoptimal modeling of SRP is currently the main source of error in determining the orbits of GNSS satellites. The complex shape of these satellites (bus and wings) combined with their particular attitude law—which requires the face of the satellite that collects the different antennas to communicate with the ground stations to continuously point to the nadir while the face near the atomic clocks must look toward deep space, and finally the array of solar panels must continuously point toward the Sun for energy reasons—make the modeling of this perturbation and its optimal insertion into the precise orbit determination (POD) process a nontrivial issue. We also underline that studies like the present one, aimed at improving the modeling of the orbits of the satellites of the Galileo constellation, are of some importance for ESA in the light of future programs that foresee the use of Galileo satellites for increasingly significant purposes, as in the fields of earth sciences (such as geodesy, geophysics, and remote sensing), fundamental physics, astronomy, and time metrology [15].

The work we describe in this paper is the first of two works that we present in this issue of the journal. These works concern some of the activities currently underway at the IAPS-INAF Institute in Roma. In particular, in this paper we will focus on the NGPs models currently developed within the GNSS community and we introduce a 3D-CAD of a Galileo FOC that we have built and that we plan to use in the near future for modeling these nonconservative forces. In this regard, the 3D-CAD will be the basis for the construction of a finite element model (FEM) of the spacecraft. Indeed, the development of the FEM requires a better knowledge of the optical and thermal properties with respect to those currently available in the Galileo metadata of the European Space Agency (ESA). In the meantime we have also developed a box-wing model for these satellites based on the information contained in the Galileo metadata of ESA. In a second paper we will present the results obtained for the direct SRP from the application of the box-wing model together with some preliminary POD for the Galileo FOC satellites.

With a view to achieving the ambitious objectives of G4S in the field of fundamental physics measurements, we underline the importance of developing a dynamic model of the main gravitational and nongravitational perturbations on the Galileo satellites which is extremely robust and reliable. This will significantly improve the determination of their orbits and related products, such as the estimation of the clock-bias of the on-board atomic clocks.

Consequently, this paper is organized in three parts. In the first we will focus on and discuss the main peculiarities and drawbacks of current models developed for the modeling of the NGPs of GNSS satellites. In the second part we provide an estimate of the accelerations due to the main NGPs as well as an estimate of their uncertainty. Finally, in the third part of the paper we introduce our preliminary models for the Galileo FOC satellites to manage the perturbing effects due to the main NGPs. To this end, the results of the analyzes on the state of the art of the NGPs models developed in the first part of this work were fundamental.

Specifically, the rest of the paper is organized as follows. In Sec. II, we first provide a classification of the main NGPs acting on GNSS satellites. In Sec. III, the state-of-the-art of the modeling of NGPs for GNSS satellites is presented together with their main criticalities. Special care is devoted to the Galileo constellation. In Sec. IV, the order-of-magnitudes of the main NGPs on Galileo FOC satellites are provided with an estimate of their corresponding uncertainties. In Sec. V, we provide our first models for the Galileo FOC satellite to be used for calculating the accelerations produced by the main NGPs. Finally, in Sec. VI our conclusions and recommendations are provided.

II. NGPs CLASSIFICATION

The improvements over time of the POD of the satellites belonging to the constellations of the GNSS, starting from the GPS one, has highlighted, since several years, the complex and subtle effects of the NGPs on their orbit and, consequently, the need to account properly for their perturbing effects to further improve the POD of these satellites at the current level of the microwave-ranging accuracy/precision [16–20]. In the case of GNSS, the management of NGPs is further complicated, as said, by the complex shape of these active satellites, compared, for example, to passive satellites, which do not have solar panels, motors and antennas. The POD improvements are truly significant for the multiplicity of products obtained from the analysis of the orbits of these satellites. These products may be classified, at a higher level, into four main categories:

(1) Positioning.
(2) Timing.

(3) Geophysics.
(4) Fundamental physics.

These high-level products are, of course, intimately linked to each other and not independent, having in common the precise knowledge of the orbits of the satellites, that is, of their ephemerides. Among the parameters that control the size of the NGPs relative to the gravitational perturbations is the area-to-mass ratio A/M of a spacecraft. In the case of an artificial satellite around the Earth this quantity is relatively high, between 0.01 and 0.001 m^2/kg, while it is several orders of magnitude smaller for a natural body (being inversely proportional to its radius for a homogeneous body with uniform density). Consequently, in the case of a natural body the NGPs are usually negligible and its motion is usually studied by celestial mechanics within the Hamiltonian formalism of conservative forces. Of course, there are a few important exceptions: as the nongravitational thrust acting on some comets and the deceleration of the Moon along its orbit around the Earth due to energy dissipation produced by the tides raised by the Moon on the Earth's seas [21,22]. Conversely, for the artificial satellites such perturbations are not negligible if their orbits are tracked very precisely, and the approaches of "dirty" celestial mechanics are necessary to account for the effects due to these nonconservative forces [23].

Indeed, there are three possible approaches to account for the perturbing effects of the NGPs on a spacecraft:

(1) Model as better as possible their complex effects.
(2) Measure with a high-sensitive accelerometer their accelerations.
(3) Use a drag-free satellite.

Within G4S_2.0 we are interested to the first two approaches. In particular, in this paper we will concentrate only in the first point. Our goal is to define the current limits of the dynamical model for the NGPs, as well as those of the best possible dynamic model that can in principle be developed for GNSS, in particular for the Galileo constellation, to manage the NGPs so as to obtain the best possible POD based on the current tracking technologies of their orbits [24–28]: i.e., microwave and satellite laser ranging (SLR) [29].

As underlined in the previous section, this activity is carried out with a view to future measurements in the field of fundamental physics that we plan to make by exploiting a better knowledge of the orbits of these satellites. However, this activity will also help us to define the main characteristics of an onboard accelerometer, such as its sensitivity and measurement bandwidth, to be considered as a new payload for a next generation of Galileo satellites to further improve the performance of the Galileo constellation.

In the following subsections, a classification of the main NGPs will be presented with the aim of defining the complex panorama of perturbative effects at play and therefore defining the strategy to be followed to take into account, through new models, of their effects on the orbit of Galileo satellites. Conversely, in Sec. III a description of the main models currently used to account for their perturbing effects will be presented.

A. Classification of the nongravitational perturbations

In the following we classify the NGPs on the Galileo satellites based on their source. In this case we need to consider three different sources:

(1) Sun.
(2) Earth and its environment.
(3) Spacecraft itself.

However, it is important to emphasize that the perturbations that result from these sources are not completely independent. For instance, just to give two important examples, the effects of the Earth's atmosphere depend significantly on solar activity and its variations, while the terrestrial albedo depends on both solar radiation and clouds cover. As is well known from the literature, the LAGEOS geodynamic satellites [30] have played and still plays a fundamental role in the fields of geophysics and space geodesy, as well as in that of fundamental physics [31–38], and numerous refined models for the NGPs acting on their surface have been developed to improve their POD results in these areas. Consequently, a comparative analysis of the state of the art between Galileo satellites (or GNSS in general) with LAGEOS satellites will be provided below whenever deemed useful.

1. NGPs due to the Sun

The perturbation of the visible solar radiation on a spacecraft may be subdivided in the following physical effects:

(1) Direct SRP.
(2) Yarkovsky-Schach.
(3) Asymmetric reflectivity.
(4) Poynting-Robertson.

The direct SRP represents the largest NGP on a satellite of the GNSS and, in principle, the "easiest" to model. The perturbation arises by the interaction of the solar light with the surfaces and elements of the spacecraft and results in a momentum transfer to the satellite. The eclipses from the Earth plays a significant role in order to correctly account for the orbital effects produced by this perturbation [23,39]. The SRP is responsible of long-term effects on the orbital elements.

The Yarkovsky-Schach effect arises by the modulation of the SRP when the satellite enters and exits from the eclipses and depends on the thermal inertia of the spacecraft surfaces and elements and by its attitude in space. This combination produces a nonuniform distribution of temperature across the satellite surface, with a resultant perturbing acceleration that does not average out during an orbital revolution and with long-term effects on the orbital

elements. This effect is well known in the case of the two LAGEOS satellites [40–50]. In the literature of GNSS, this perturbation is not explicitly considered, at least in the above description, but falls (in part) within the thermal reradiation from the spacecraft.

The Asymmetric reflectivity arises from a possible difference in the reflectivity of the various part of the satellite and it depends on the attitude of the satellite. This effect has been investigated in the past in the case of the two LAGEOS satellites [43,44,47,50–53].

The Poynting-Robertson effect [54–56] arises from the reradiation of the solar light absorbed by the spacecraft and assumed to be reradiated isotropically in its own frame of reference. The light emitted in the direction of motion is blue shifted and carries away more momentum and energy than the light emitted in the opposite direction, consequently a reaction force appears that decelerate, in principle, the spacecraft. In the case of LAGEOS this effect was investigated by [40].

2. NGPs due to the Earth and its environment

The perturbations due to the Earth and its environment may be subdivided in the following physical effects:

(1) Albedo.
(2) Infrared radiation pressure.
(3) Neutral drag.
(4) Charged drag.
(5) Earth-Yarkovsky.
(6) Poynting-Robertson.

The main effects on the orbit of a spacecraft are due to the indirect SRP, i.e., to the Earth's albedo perturbation, and to the infrared radiation pressure. The perturbation arises by the interaction of the visible solar light with the Earth's surfaces and its complex anisotropic reflection.

In the case of a satellite in a low Earth orbit (LEO) the perturbing effects of the neutral atmosphere are significant and may compete with the perturbations due to the albedo and even with those due to the direct SRP. Again, the eclipses of the satellite play a significant role in the analysis of almost all these effects [23,57].

In the case of the radiation coming from the Earth, while the direct effects of the infrared radiation (long-wavelengths) may well be approximated by a few zonal harmonics (i.e., with no longitudinal dependency) [58], the day/night asymmetry makes this more difficult for the albedo, i.e., for the visible radiation which is reflected and diffused by the Earth's surface and atmosphere. Actually, the intensity and direction of the force are complex functions of position and time, since the local optical behavior of the Earth's surface and atmosphere is highly variable, related both to surface composition and morphology and to meteorological and seasonal effects [59].

Therefore, long-term effects of the albedo perturbation on a satellite are complex and subtle, since they depend in a critical way on the asymmetry between the Earth's northern and southern hemispheres, resulting both from the different sea/land distribution and from seasonal phenomena (e.g., cloud and snow cover). In particular, the anisotropically reflected radiation (i.e., not symmetrically distributed around the local zenith) from a surface element (especially in the case of oceans), produces long-term effects on the satellite orbit. In the case of the two LAGEOS a very reach literature on this subject has been produced [40,47,50,51,57,60–64].

In the case of GNSS, the albedo perturbation represents the most important, in magnitude, to be considered after the direct SRP [65,66]. However, Earth radiation data from dedicated satellites—in different band of the spectrum, from long-waves flux to short-waves flux—allows us to improve the modeling of both the Earth's visible and infrared radiation. In particular, data from the CERES (Clouds and the Earth's Radiant Energy System) [67] database are extensively used in the literature.

The neutral drag perturbation is due to the collisions between the satellite and the particles of the Earth's atmosphere along its trajectory. In the case of LAGEOS-type satellites this perturbation has been well investigated in the literature [40,68–71]. As previously underlined, the neutral drag perturbation represents a very important effect for LEO satellites [72], but may be fully neglected for GNSS, because of their high altitude.

The interaction of a spacecraft with the surrounding atmosphere is not limited to the direct collisional effects with the particles but also to possible charged drag effects. These arises by the interaction of a charged satellite with the particles of the plasmasphere. Indeed, as consequence of the Earth's magnetic field, the Earth's is surrounded by a toroidal region where charged particles are trapped to move under the Lorentz force. Consequently, a charged drag arises due to the Coulombian interaction between the charged satellite and the charged particles. This kind of effect is strongly influenced by the eclipses, because of the corresponding variation of the photoelectric effect produced by solar radiation. While this effect has been investigated in the case of the LAGEOS satellites [40,50,68,70,73], it seems that this effect has never been considered in the GNSS literature.

Similarly to the Yarkovsky-Schach effect, the Earth-Yarkovsky effect arises from the anisotropic distribution of temperature produced on the satellite by Earth's radiation, in particular from infrared radiation. The effect depends from the thermal inertia of the satellite surface, in particular from the corner cubes retroreflectors (CCRs), and from its attitude in space [49,73,74].

The Poynting-Robertson is the same as that described in previous section but produced by the Earth's radiation [40].

3. NGPs due to the spacecraft

An active spacecraft, such as one of the GNSS, is itself responsible for producing NGPs of thermal origin.

The knowledge of the overall temperature distribution of the satellite is therefore of fundamental importance to account correctly for this kind of effects. Moreover, in addition to these thermal accelerations we must consider the thrust acceleration produced by the antennas and by maneuvers. Consequently, following the main literature in this field [75–78] we can consider the following main disturbing sources:

(1) Radiation of thermal blankets.
(2) Radiation from the radiators.
(3) Solar panels thermal radiation.
(4) Thermal radiation of excess solar array power (shunt).
(5) Antennas radiation.
(6) Maneuvers.
(7) Mass variation.
(8) Sloshing.

For the GPS block IIR satellites it was pointed out [77] that: "The solar array and shunt thermal radiation forces are the next lowest, representing just under 1 percent of the total each, but provide a nearly constant value about the orbit. Although the magnitudes are similar, these forces are applied in opposite directions and nearly cancel each other out," therefore, considering these thermal perturbations explicitly negligible with respect to the direct and indirect solar radiation pressure. Following [77] in the case of GPS block IIR the following explanation was given:

(1) Radiation of thermal blankets:
   (i) Exterior body blankets absorb solar radiation and immediately reradiate it back to space, preventing excessive heating of the vehicle. The reradiation is diffuse emission of the absorbed radiation. The process of absorption and reradiation is equivalent to diffuse reflection. The surface body properties are adjusted to model reradiation as diffuse reflectivity and the results are included with the visible solar forces instead of the thermal forces.
(2) Radiation from the satellite radiators:
   (i) Space vehicle internal components generate heat that must be dumped to space to prevent excessive temperatures.
(3) Solar panels thermal radiation
   (i) The solar arrays and shunt dissipaters require special modeling due to the conversion of electrical power. The reradiation force accounts for the solar array radiating heat from both the front and back sides.
(4) Thermal radiation of excess solar array power (shunt)
   (i) The shunt energy dissipation is the difference between the energy provided by the array and the energy required by the on-board subsystem components. The shunt force is calculated from this dissipated power. The shunts dissipate energy from the anti-Sun side only.
(5) Antennas radiation
   (i) RF radiation force is included with the radiator forces as a steady state force throughout an orbit.
(6) Maneuvers
   (i) Reference [77] mentioned the maneuvers, but with no direct consideration of their effects.

Currently, to our knowledge, in the case of Galileo satellites, there are no dedicated in-depth studies for the above effects. Only, point 1. is usually taken into consideration in the way suggested by [77]. However, even in the case of GPS satellites, the studies mentioned above cannot be considered exhaustive, as they are characterized by simplifications and approximations, sometimes unavoidable, and the models developed are mainly based on empirical terms.

As specified above, active satellites, such as GNSS satellite, have antennas emitting a significant radiated power. In this case the spacecraft is also affected by a thrust due to antenna, the so-called antenna thrust, a small acceleration pointing into the direction opposite to the antenna. Indeed, the transmission of GNSS navigation signals is carried out by sending microwave power toward the Earth by the antenna. Being typically fixed for GNSS (Galileo as well [79]), the boresight of the antenna must always be directed toward the Earth's center to provide a correct signal strength (i.e., the navigation message) and an optimized coverage. In order to evaluate such an effect, the knowledge of the transmitted power and the spacecraft mass are requested, in addition to the orbit height. Indeed, the modeling of such a term can be carried out as follows, according to [23]:

$$\mathbf{a}_{\text{thrust}} = \frac{P}{Mc}\frac{\mathbf{x}}{|\mathbf{x}|} \tag{1}$$

where P is the transmitted power, M is the spacecraft mass, c the speed of light in vacuum, and $\mathbf{x}$ is the position vector of the satellite. In this modeling it is assumed that the antenna boresight is directed toward the Earth's center and the antenna has a radiation pattern with a narrow-beam and a rotationally symmetric gain [80].

All the aspects mentioned above will need to be deepened and well defined when it becomes necessary to develop a reliable thermal model of the satellite. For this to be indispensable, optimal modeling not only of the direct solar radiation pressure, but also of the albedo and terrestrial infrared radiation must be achieved.

III. NGPs MODELS FOR GNSS SATELLITES

Considering the NGPs modeling, two main approaches may be considered:

(1) Build a refined model for the spacecraft in such a way to compute the effect of the interaction of each surface element, as well as of the appendices,

with the external (or even internal) radiation sources. The corresponding perturbing accelerations will be used in the POD for the data reduction.

(2) Apply the tools of celestial mechanics to find which component of the perturbing force is really significant, on the basis of the tracking technique and time of accumulation of its effects on the orbit. Develop an analytic model (usually a simplified model) to be included in the dynamical model used in the POD for the data reduction.

In this section these two approaches will be considered and described in their guiding elements on the basis of the state of the art of the literature and of the POD procedures typical of GNSS. Our main objective in this context is to build, on the basis of the information collected, a new finite element model (FEM) of the Galileo FOC satellites (see Sec. V) that can meet the ambitious objectives of G4S_2.0: that is to improve the POD of the satellites in order to use their orbits for fundamental physics measurements.

A. General aspects

Usually, in the literature of the NGPs modeling, the second approach has been followed, by fixing some of the parameters of the model (these are "considered parameters") and estimating the other in the POD, as for the radiation coefficient C_R or the drag coefficient C_D (these are adjusted parameters). Sometimes, these analytical models are accompanied by the use of empirical accelerations to better absorb some effects not currently modeled [16,81–84], as in the case of the empirical CODE orbit model (ECOM) and its subsequent versions. In a few cases also stochastic accelerations or velocities are introduced to absorb the orbit mismodeling.

Certainly, the use of empirical accelerations does not allow to obtain a physical description of the many perturbative effects involved. Therefore, such empirical accelerations must be introduced with extreme care when it is deemed necessary, and with the main objective of reducing the orbital residuals in the POD of the satellites. Anyway, their use should be avoided whenever the correct physical interpretation of a given effect is requested, as for instance in the case of the origin of the so-called Y-bias acceleration or when fundamental physics measurements are considered.

Presently, the best representation of the second approach can be considered a simple (or simplified) box-wing (S-BW) model. With a S-BW model we mean the consideration of a number of flat surfaces of the spacecraft through which we are able to estimate the SRP accelerations acting on it, once the average optical coefficients of each surface have been set. Of course, at the same time, the development of a BW model represents a first step toward the realization of the first approach previously cited, i.e., the development of a FEM for the satellite. The development of a really refined FEM requires:

(1) A very accurate representation of the complex geometry of the spacecraft.

(2) The knowledge of the physical characteristics—such as optical (in the visible and in the infrared) and thermal—of each kind of surface and element (antenna, appendices, CCR, insulators, radiators, etc.) that constitute the spacecraft, also including the internal ones.

(3) The knowledge of how these characteristic (especially the optical ones) evolve in time and how they are function, for instance, of the illumination conditions.

(4) To account for multiple reflections.

(5) The knowledge with high accuracy of the spacecraft attitude with respect to the Earth and to the Sun during its orbital revolution around the Earth, as well as during the (unavoidable) orbital maneuvers.

(6) For a given attitude, we need to be able to model the mutual shadowing effects produced by the spacecraft surfaces and appendices, in order to account for umbra and penumbra effects.

Consequently, the development and fruitful use of a refined and complete FEM of a spacecraft, based on the application of the ray-tracing technique, is a truly daunting task. In fact, until the last years, this first approach in modeling has not been pursued, due to the numerous complexities mentioned above, and also due to the numerical integration and the time required to perform all the detailed interactions, which must include multiple reflections, with umbra and penumbra calculations, the knowledge of the optical properties of the surfaces and the correct satellite attitude in space. Consequently, the $\approx 1\%$ precision reachable (in principle) in the modeling of the direct solar radiation pressure by means of a reliable FEM was indeed considered illusory [23], also in relation to the lower quality of tracking in the past.

However, in the last two decades, thanks to the improvements in computing power, together with the development of algorithms and dedicated software for ray-tracing techniques, or by test particle Monte Carlo (TPMC) approach [85–88], even with a normal *personal computer* it is now possible to produce a satellite FEM able to improve the modeling of NGPs, starting from the SRP, the largest NGP on GNSS spacecraft.

Indeed, first, as previously introduced, several BW models have been developed—with different (but still limited) level of sophistication—for GNSS spacecraft [17,66,89–92] and, in particular for the Galileo ones [20,93–95].

Regarding the construction of a FEM, this possibility has been considered in numerous papers in the GNSS literature to improve the modeling of the SRP and secondly of the thermal effects [17,75,76,89,90,93,94,96–99]. However, although the main ingredients for developing a reliable FEM have been well highlighted in the cited literature, especially in the most recent works, it seems that a refined FEM has never been developed and tested and routinely

applied in the POD of GNSS satellites, or at least the corresponding results and applications have never been published. We think this is closely related to how the so-called *precise orbits* are currently determined by the International GNSS Service (IGS). These are in fact, together with the *clock-bias*, one of the main products that today are obtained from the analysis of the orbits of GPS and GLONASS satellites. Since these are determined over a short time interval, the NGPs perturbations do not have time to accumulate sufficiently and what is not modeled is absorbed by estimating empirical terms. We will return to these aspects later, see Secs. III B 2 and III B 5.

Concerning the use of a FEM for Fundamental Physics applications and, in particular, in the case of the measurement of the gravitational redshift, both ZARM and SYRTE have done some activity in this direction. Indeed, a FEM of a Galileo FOC has been developed by ZARM and the results for the SRP have been used by ESA in their POD for the measurement of the gravitational redshift performed in 2018 [7], but no results have been published in this regard at the time of this measurement (Benny Rievers personal communication) and no mention of the FEM is reported in [7]. The FEM model developed by ZARM was published only in 2023 [100]. This model has good performance, well superior to those of a S-BW, but cannot be considered a refined FEM of the Galileo FOC satellite since not based on sufficiently detailed information regarding the optical properties of the various components of the satellite and also not having any information on the temperature distribution on the satellite (Benny Rievers personal communication). Consequently, the accuracy that can be achieved with a FEM for modeling the SRP for a Galileo FOC satellite has not yet been defined. However, the quality of the FEM described in [100] is remarkable under several aspects.

In the case of the measurement of the gravitational redshift performed by SYRTE [8], in their supplementary material [101] it is explicitly written: *For direct and indirect solar radiation pressure (SRP) modeling of the Galileo FOC (full operational capability) satellites, a numerical raytracing model based upon the geometrical form of the surface of the spacecraft and the optical characteristics of each component is employed*. The authors refers, quoting the Ref. [102], to the software Aerodynamics and Radiation Pressure Analysis (ARPA) developed at the University of Padua in Italy for the analysis of the nongravitational forces acting on GOCE [103]. Again, there is no clear explanation for the quantitative improvement in the POD of a Galileo FOC satellite using such software over the usual models.

B. Current main models for the NGPs

Based on the extensive literature of satellites belonging to the GNSS, and also regarding the analysis of their orbits for applications in the fields of geophysics and space geodesy, as for:

(i) Earth rotation parameters.
(ii) Global scale.
(iii) Geocenter coordinates.

See for instance [104,105], we can summarize the current models for the NGPs in the following typologies (also following a chronological order in their development):

(1) Cannonball.
(2) Empirical accelerations.
(3) Pseudo stochastic pulses.
(4) S-BW.
(5) BW with empirical accelerations.
(6) BW with adjusted coefficients.
(7) FEM.

1. Cannonball model

The cannonball model represents a very rough solution to take into account the shape of a satellite. In the case of the SRP, it models the average cross section seen by the Sun and with average optical coefficients parametrized by a radiation coefficient (of course, the cross section seen by the Earth is different from this average value, because of the solar panels orientation toward the Sun, and it is subject to a periodic variation). The cannonball model accounts for the average (bulk) acceleration on the spacecraft but with a low spectral content, practically only for an effect at the orbital period of the spacecraft. Therefore, many features are lost when using a simple cannonball model. In the case of GPS literature, it was usually used as an *a priori* model complemented by estimates of empirical terms along the axes of the spacecraft (+Z toward the Earth, +X toward the half plane that contains the Sun, and +Y completes the right-handed system and point along the solar panels axis).

We refer to the accompanying paper for the application of the cannonball model to the POD of the Galileo FOC satellites.

2. Empirical models

In the literature of GNSS, starting from GPS and GLONASS, the empirical models have been, and still are, very successful to account for the SRP perturbation [16,82]. The empirical model is based on the results acquired at the center of orbit determination in Europe (CODE) since 1992 in the context of several activities regarding the IGS. Within CODE the direct SRP acceleration is modeled as:

$$\mathbf{a}_{\odot} = \mathbf{a}_{\odot,\mathbf{0}} + D(u)\hat{\mathbf{s}} + Y(u)\hat{\mathbf{e}}_{\mathbf{Y}} + X(u)\hat{\mathbf{e}}_{\mathbf{X}}. \qquad (2)$$

The first term, $\mathbf{a}_{\odot,\mathbf{0}}$, represents the acceleration as given by an *a priori* model for the SRP (usually the ROCK model used by GPS, see, e.g., [76,106]), $\hat{\mathbf{s}}$ is the unit vector from the spacecraft center of mass to the Sun (indicated as $\hat{\mathbf{e}}_{\mathbf{D}}$ in [16]), $\hat{\mathbf{e}}_{\mathbf{Y}}$ is the unit vector along the spacecraft solar panel axis, $\hat{\mathbf{e}}_{\mathbf{X}} = \hat{\mathbf{e}}_{\mathbf{D}} \times \hat{\mathbf{e}}_{\mathbf{Y}}$ defines a right-handed reference system,

and u represents the argument of latitude of the spacecraft ($u = \omega + f$, with ω the argument of pericenter and f the true anomaly). Each of the accelerations terms $D(u)$, $Y(u)$ and $X(u)$ represents an empirical acceleration constituted by a constant and two periodic once-per-revolution accelerations (sine and cosine terms):

$$\begin{cases} D(u) = D_0 + D_s \sin u + D_c \cos u \\ Y(u) = Y_0 + Y_s \sin u + Y_c \cos u \\ X(u) = X_0 + X_s \sin u + X_c \cos u \end{cases} \tag{3}$$

Therefore, this model contains up to nine parameters that can be estimated over a fixed time span in order to absorb the unmodeled part of the SRP perturbation, see also [104]. More recently, the ECOM model was extended to ECOM2 [18]. The ECOM2 model considers a constant acceleration along each of the above axis, plus even periodic terms in the Sun direction (currently, twice-per-revolution terms) and odd periodic terms along the X axis (currently, once-per-revolution terms). Consequently, Eq. (3) transforms as:

$$\begin{cases} D(u) = D_0 + \sum_{i=1}^{n_D} \{D_{2i,c} \cos 2i\Delta u + D_{2i,s} \sin 2i\Delta u\} \\ Y(u) = Y_0 \\ B(u) = B_0 + \sum_{i=1}^{n_B} \{B_{2i-1,c} \cos(2i-1)\Delta u + B_{2i-1,s} \sin(2i-1)\Delta u\} \end{cases} \tag{4}$$

where we have introduced the symbol B instead of X, following the notations of [18], and where the argument of latitude $\Delta u = u - u_\odot$ of the satellite with respect to that of the Sun has replaced the argument of latitude u of the satellite. It is important to stress that the B-axis does not coincide (in general) with an axis of the spacecraft, and so it does not correspond to the orientation of the spacecraft bus; it varies in a space limited by the $\pm Z$ and $+X$ axes.

3. Pseudostochastic pulses

The so called pseudo-stochastic pulses were firstly introduced by [16] and allow to estimate instantaneous velocities changes of a satellite in predefined directions (usually radial, cross-track and transverse directions) at predefined epochs. This method was later generalized to allows for piecewise constant or even piecewise linear accelerations [107,108] in the POD. In the data reduction, the pseudostochastic pulses are treated as any other adjusted parameter; consequently, since the partial derivatives of the orbit are needed with respect to these additional parameters, the normal equations may grow considerably in their size, leading to a not efficient least-squares procedure [25].

4. Box-wing model

Several box-wing models, as already highlighted, have been developed for GNSS satellites. In the case of the Galileo FOC we refer to [20,95] that have built a S-BW on the basis of the Galileo metadata [109] and following [17]. The BW is obtained by considering the satellite, as a box made of flat surfaces (such as a parallelepiped or a cuboid) plus the flat wings of the solar panels. Assuming that each surface dA behaves like a linear combination of a black body, a perfect mirror and a perfect diffuser—with the corresponding optical coefficients: α (for absorption), ρ (for specular reflection) and δ (for diffuse reflection), and such that $\alpha + \rho + \delta = 1$—for the acceleration produced by the direct SRP we obtain the following expression [23]:

$$\mathbf{da} = -\frac{\Phi_\odot}{Mc}\left[(1-\rho)\hat{\mathbf{e}}_\mathbf{D} + 2\left(\frac{\delta}{3} + \rho\cos\vartheta\right)\hat{\mathbf{n}}\right] dA|\cos\vartheta| \tag{5}$$

where $\Phi_\odot$ represents the solar irradiance, M the mass of the satellite, c the speed of light, $\hat{\mathbf{n}}$ the unit vector normal to the surface dA and ϑ the Sun zenith angle with respect to the surface normal: $\cos\vartheta = \hat{\mathbf{e}}_\mathbf{D} \cdot \hat{\mathbf{n}}$.

The condition $\alpha + \rho + \delta = 1$ represents a strong assumption, which means that the absorbed light is not reemitted, that the light reflection is perfectly specular and, finally, for a given direction the intensity of the diffused light is proportional to the cosine of the angle with the normal $\hat{\mathbf{n}}$, i.e., Lambert's law holds up with a diffusion lobe of spherical shape. In the case of the model described in [20,95], as well as in [17], Eq. (5) in the case of the bus was replaced by:

$$\mathbf{da} = -\frac{\Phi_\odot}{Mc}\left[(\alpha+\delta)\left(\hat{\mathbf{e}}_\mathbf{D} + \frac{2}{3}\hat{\mathbf{n}}\right) + 2\left(\frac{\delta}{3} + \rho\cos\vartheta\right)\hat{\mathbf{n}}\right] dA|\cos\vartheta|, \tag{6}$$

following the suggestion of the authors of [77], i.e., assuming immediate thermal reradiation. In this case, we need to consider an additional contribution to the acceleration given by the radiation that is radiated back to space according to Lambert's law:

$$\mathbf{da}_{rr} = -\frac{2}{3}\alpha\frac{\Phi_\odot}{Mc} dA|\cos\vartheta|\hat{\mathbf{n}}, \tag{7}$$

which added to Eq. (5) gives Eq. (6). However, by doing so, the validity of the previous condition:

$$\alpha + \rho + \delta = 1 \tag{8}$$

is still imposed, but in reality it is no longer valid in the case of reemission of the absorbed radiation.

As for the NGPs, the authors of [20,95] have applied their BW model to the direct SRP, the Earth's albedo and infrared radiation and the thrust produced by the navigation antenna. The POD results for this S-BW model were compared with hybrid box-wing solutions, where a set of empirical parameters, following the ECOM and ECOM2 style, where estimated in order to reduce the orbit residuals. In this way, the authors were able to obtain the best solution for their POD, as well as for orbit predictions and for estimating geodetic parameters.

Finally, by means of a BW model it is possible to adjust, in the POD procedure, some of the optical coefficients of the surfaces with the goal to reduce the orbital residuals of the satellites. This can be useful if the information on the optical properties is not reliable or considered not updated. Indeed, this approach was followed in part by [17] for the GPS satellites (Block II/IIA and IIR) during a dedicated analysis in 2007. The tracking data of the GPS were obtained from CODE and two different solutions computed: (i) one using the adjustable BW model and (ii) one using the empirical model of CODE. The analyses performed for the year 2007 focused on the difference between the estimated parameters and orbits in the two cases.

5. Finite element model

The main features of a refined FEM have already been introduced in the previous Sec. III A together with the numerous difficulties in its reliable implementation. In the following, we are interested in highlighting some of the advantages that can be obtained in the future for GNSS satellites through the use of a reliable FEM:

(1) A new high-precision numerical model to account for the perturbative effects of direct SRP allows to avoid the strong use that is currently being made of empirical parameters during the POD.
(2) It would allow better modeling of perturbative effects that are two orders of magnitude lower in acceleration than SRP, starting from Earth's albedo and infrared radiation pressure.
(3) It would pave the way for a better and more detailed consideration of the numerous thermal reradiation effects previously introduced, see Sec. II A.
(4) It would hopefully allow, under favorable conditions, to take into account the perturbative effects linked to the variation of solar irradiation.
(5) it would allow to provide (both directly and indirectly) better predictions for the orbits generated by IGS and by the main analysis centers.
(6) it would allow to provide a more precise and accurate POD for the fundamental physics applications of GNSS satellites.

Regarding the first point, the physical reasons that suggest, possibly, to avoid an intensive use of empirical terms in the POD have already been highlighted in Sec. III B. In fact, in addition to drastically reducing its use, the FEM could limit the use of empirical terms to perturbative effects in acceleration much smaller than those produced by direct SRP.

In particular, a successful application of FEM to modeling the effects of radiation pressure from the Earth-atmosphere system, second point above, would limit the use of empirical terms to thermal effects.

As for the third point, in case we have a good knowledge of the temperature distribution on the surface of the spacecraft and its elements (also considering its interior, with heat transport and radiation mechanisms of the spacecraft structure)—distribution that strongly depends (but not only, see Sec. II A) from the illumination of the Sun—it would be possible in principle to calculate the elementary acceleration from each surface element. This would allow us to calculate the total acceleration produced by the radiation emitted by the spacecraft's surface due to its anisotropic temperature distribution. We refer to [98] as a very good example in this direction.

Concerning the solar irradiance (point four), it is estimated to vary in the range $0.1\% \div 0.2\%$ during one solar cycle of about 11 years. Its contribution to the model uncertainty are currently negligible with respect to the error that arises from the knowledge of the optical coefficients of the Galileo FOC satellites, and in general of the GNSS ones. Therefore, its *a posteriori* modeling will be possible and fruitful only if, before the launch of a satellite, precise measurements of the optical coefficients of the various surfaces and elements, and in particular of the solar panels, will be made. In this regard, the law of degradation of the optical coefficients and the knowledge of the satellite's attitude will also play a significant role.

Today, the measurement uncertainties of the solar irradiance are comparable with its variations over the solar cycle. The irradiance variations are measured through radiometers onboard dedicated satellites since 1978. These measurements show a well-defined correlation between the 11-year solar cycle and the solar magnetic activity cycle [110].

The timescales on which the solar irradiance varies are different depending on the physical cause that is at the origin of the variation in the irradiance itself. If we restrict to irradiance variations at timescales up to the solar cycle, of the order of a lifetime of a typical GNSS constellation, we can highlight the following timescales:

(i) From minutes to hours: the variability is driven by p-modes (i.e., pressure modes due to standing sound waves) and granulation (i.e., due to convenction

cells in the convective zone below the Sun's photosphere).

(ii) From hours to days: the variability is mainly driven by sunspots (i.e., by the evolution and rotational modulation of magnetic features) and granulation or supergranulation.

(iii) From days up to $\simeq$1 month (about the Sun rotation period) [111]: the variability is mainly driven by sunspots and faculae (i.e., by bright spots in the photosphere).

We refer to [112,113] for further details on the solar irradiance and its variations.

Currently, considering the magnitude of the variation in solar irradiation and also considering that the limit of a precision of 1% of a SRP model based on an FEM is in any case a very difficult task to achieve and also to maintain over time, probably the corresponding variations of the acceleration due to direct SRP, on the order of a few 10^{-10} m/s^2, will be very difficult to model correctly. This is a case where the measurements of an accelerometer with the right sensitivity could perform better than present, and possibly future, models.

As for the fifth point, a reliable model for the SRP is crucial for providing more reliable predictions for the orbits of the satellites. In fact, the goodness and reliability of this model is one of the main aspects that influence the final accuracy of the predicted orbits by the IGS. Indeed, predictions, i.e., orbit propagation, represents an important issue in the current activities of the IGS.

A very good example is provided by ultrarapid orbits, that are very important for real-time or *quasi* real-time applications. In this case the orbits are determined by a fit of the observations (i.e., of the phase of the carrier) on a period of three days. The state vector of the satellite is estimated at the beginning of the first day.

The ultrarapid orbit is provided on two days files as follows: the first day consists of the observed orbit during the third daily arc, obtained by propagating the estimated state vector at the beginning of the arc of the first day; the second day of the ultrarapid orbit consists of a predicted orbit (or propagated orbit) after the third day of the POD, it corresponds to the fourth day. Than the POD process is repeated with a 6-hour shift. These are combined orbits, for the first day orbit the accuracy is about 3 cm, while for the fully predicted orbit the accuracy is about 5 cm. Clearly, in all these orbit propagation contexts, reliable models and their covariance play a crucial and irreplaceable role.

On the contrary, the measurements of an accelerometer, as well as the use of empirical terms, cannot provide a direct contribution to the prediction of the orbit. However, an indirect effect is possible. Indeed, the measurements of the on-board accelerometer can be used to calibrate some parameters of the NGPs models, as well as some empirical terms.

The last point is the one we are most directly interested in. Of course, once a reliable FEM has been implemented, and with the most efficient approach of Ray-Tracing technique for our goals—being primarily interested in the analysis of the orbits over relatively long periods, in order to enhance (the unmodeled) relativistic effects of the secular type—the *a posteriori* analysis of the orbits is simpler than that necessary to obtain the orbits according to the procedure adopted by IGS. In this context it will be important to correctly define the length of the orbital arc of the POD of the considered satellites. This will be a function not only of the relativistic effect that is the subject of our analysis from time to time, but also of the number of observations available as regards the satellite laser ranging (SLR) technique. Indeed, full rate SLR data can be exploited to improve the orbit modeling during penumbra transitions.

However, we also believe that a study dedicated to understanding how to insert the values of perturbative accelerations of nongravitational origin, obtainable from a reliable FEM, into the POD procedures typical of GNSS analysis centers, is necessary and important.

In conclusion, by means of a reliable box-wing (R-BW) model and, hopefully in the future, by means of a FEM, it is possible to explain in principle a significant fraction of the disturbing effects that have been discussed above for the GNSS satellites and, in particular, for the Galileo ones.

Of course, the main objective still deals with the one to improve the model for the SRP and, subsequently, that for the albedo perturbation.

IV. ORDERS OF MAGNITUDE FOR THE NGPs

As already highlighted, a GNSS satellite is subject to a very wide range of physical perturbations of nongravitational origin in addition to those of gravitational origin. The latter are mainly due to the deviations of the Earth's mass distribution from the spherical symmetry and to third body effects. Even the values assumed by the various perturbative accelerations are very spread, varying on several orders of magnitude. In this context, the way to decide which perturbations are negligible is not so simple in general. An acceleration is not negligible in itself, but, firstly, with respect to the other accelerations and, second, with respect to the precision that can be achieved in the data reduction, i.e., in the satellite's POD. The POD is a function of the precision of the tracking observations of the position of the satellite, of the overall dynamical model included in the software used for the orbit determination and of the arc length used for the data reduction [114]. Of course, the main motivation for providing better (and even new) models for the various perturbations is connected with the significant increase in the precision of the tracking measurements of the satellite that have been nowadays reached, both for microwaves and (especially) for the laser

TABLE I. Comparison of the main gravitational accelerations (S.I. units) on LAGEOS II with the corresponding accelerations on a Galileo FOC satellite.

Physical effect	Formula	Parameter	LAGEOS II	Galileo FOC
Earth's monopole	$\frac{GM_\oplus}{r^2}$	$GM_\oplus = 3.986004418 \times 10^{14}$	2.6948	0.4549
Earth's oblateness	$3\frac{GM_\oplus}{r^2}(\frac{R_\oplus}{r})^2\bar{C}_{2,0}$	$\bar{C}_{2,0} = -4.841694573200 \times 10^{-4}$	1.08×10^{-3}	3.1×10^{-5}
Low-order geopotential	$3\frac{GM_\oplus}{r^2}(\frac{R_\oplus}{r})^2\bar{C}_{2,2}$	$\bar{C}_{2,2} = +2.439374598584 \times 10^{-6}$	5.4×10^{-6}	1.5×10^{-7}
Low-order geopotential	$7\frac{GM_\oplus}{r^2}(\frac{R_\oplus}{r})^6\bar{C}_{6,6}$	$\bar{C}_{6,6} = +9.476848430257 \times 10^{-9}$	3.7×10^{-9}	3.0×10^{-12}
High-order geopotential	$13\frac{GM_\oplus}{r^2}(\frac{R_\oplus}{r})^{12}\bar{C}_{12,12}$	$\bar{C}_{12,12} = 2.422093764787 \times 10^{-9}$	3.7×10^{-11}	1.4×10^{-16}
Moon	$2\frac{GM_\bullet}{r_\bullet^3}r$	$GM_\bullet = GM_\oplus/81.3$	2.2×10^{-6}	5.3×10^{-6}
Sun	$2\frac{GM_\odot}{r_\odot^3}r$	$GM_\odot = 1.32712442099 \times 10^{20}$	9.6×10^{-7}	2.3×10^{-6}
Venus	$2\frac{GM_\varphi}{r_\varphi^3}r$	$GM_\varphi = 0.82GM_\oplus$	1.2×10^{-10}	3.0×10^{-10}
Indirect oblation	$3\frac{GM_\oplus}{r_\bullet^2}(\frac{R_\oplus}{r_\bullet})^2\frac{M_\bullet}{M_\oplus}\bar{C}_{2,0}$	$GM_\oplus, \bar{C}_{2,0}$	1.4×10^{-11}	1.4×10^{-11}
Dynamic solid tide	$3k_2\frac{GM_\bullet}{r_\bullet}(\frac{R_\oplus}{r_\bullet})^2\frac{R_\oplus^3}{r^4}$	$k_2 \simeq 0.3$	3.9×10^{-8}	1.1×10^{-9}
Dynamic ocean tide	≈0.1 of dynamic solid tide		3.9×10^{-9}	1.1×10^{-10}
Kinematic solid tide	$h(\frac{2\pi}{T_{syn}/2})^2$	$h \simeq 0.30$	5.8×10^{-7}	5.8×10^{-7}
Kinematic ocean loading	$h_L(\frac{2\pi}{T_{syn}/2})^2$	$h_L \simeq 0.05$	9.7×10^{-8}	9.7×10^{-8}
Main GR correction	$\frac{GM_\oplus}{r^2}\frac{GM_\oplus}{c^2}\frac{1}{r}$	$\frac{GM_\oplus}{c^2} = 4.43502804 \times 10^{-3}$	9.8×10^{-10}	6.8×10^{-11}

ranging ones. A possible alternative is to measure the nongravitational accelerations with an onboard accelerometer. However, from a general point of view, it is important to underline that the accelerometer measurements must be considered as a complement to the models in a synergistic approach and, consequently, should not replace the models.

In Tables I and II are shown the order-of-magnitude of the perturbing accelerations for the current Galileo FOC satellites (column 5) due to the main gravitational perturbations and the main NGPs that we have described above. Indeed, for completeness, the NGPs accelerations are compared with the Earth's monopole acceleration and with the main gravitational accelerations. We also considered third-body effects and tides. The comparison is also extended to LAGEOS II (column 4), one of the best tracked satellites by the International Laser Ranging Service

TABLE II. Comparison of the main nongravitational accelerations (S.I. units) on LAGEOS II with the corresponding accelerations on a Galileo FOC satellite. The symbol $(\cdots)$ means that the acceleration is negligible, while the symbol $(\neg)$ means that the acceleration is currently unknown (not available), since it has not yet been evaluated.

Physical effect	Formula	Parameter	LAGEOS II	Galileo FOC
Direct SRP	$C_R\frac{A}{M}\frac{\Phi_\odot}{c}$	$\Phi_\odot = 1360.8$	3.2×10^{-9}	1.0×10^{-7}
Earth's albedo	$2\frac{A}{M}\frac{\Phi_\odot}{c}A_\oplus\frac{\pi R_\oplus^2}{4\pi r^2}$	$A_\oplus \approx 0.3$	1.3×10^{-10}	7.0×10^{-10}
Earth's infrared radiation	$\frac{A}{M}\frac{\Phi_{IR}}{c}\frac{R_\oplus^2}{r^2}$	$\Phi_{IR} \approx 240$	1.5×10^{-10}	1.1×10^{-9}
Neutral drag	$\frac{1}{2}C_D\frac{A}{M}\rho V^2$	$C_D \simeq 4.0, \rho \approx 5.7 \times 10^{-18}$	2.6×10^{-13}	$\cdots$
Charged drag	[50], Chap. 5	Species densities, floating potential	2.0×10^{-12}	$\neg$
Power from antennas	$\frac{P}{Mc}$	$P = 265$		1.2×10^{-9}
Solar Yarkovsky-Schach	$\frac{16}{9}\frac{A}{M}\frac{\epsilon\sigma}{c}T_0^3\Delta T$	$\epsilon, T_0, \Delta T$	1.0×10^{-10}	$\neg$
Earth Yarkovsky	$0.41\frac{4}{9}\frac{A}{M}\frac{\epsilon\Phi_{IR}f_0}{\alpha c}\frac{R_\oplus^2}{r^2}$	$\Phi_{IR} \approx 240, f_0 \approx 0.30, \alpha \approx 1.789$	2.5×10^{-11}	$\neg$
Asymmetric reflectivity	$\frac{1}{4}\frac{A}{M}\frac{\Phi_\odot}{c}\delta_a$	$\delta_a \simeq 0.015$	1.2×10^{-11}	$\neg$
Poynting-Robertson	$\frac{1}{4}\frac{A}{M}\frac{\Phi_\odot}{c}\frac{R_\oplus^2}{r^2}\frac{v}{c}$	$\Phi_\odot = 1360.8$	4.2×10^{-15}	1.9×10^{-14}
Thermal effect solar panels	$\frac{2}{3}\frac{\sigma}{c}\frac{A}{M}(\epsilon_1 T_1^4 - \epsilon_2 T_2^4)$	$\epsilon_1 \simeq \epsilon_2 \approx 0.8, T_1 \simeq 317, T_2 \simeq 318$		1.9×10^{-10}
Y-bias	Y_0: empirical acceleration	Y_0		7.0×10^{-10}

TABLE III. LAGEOS II and Galileo FOC mean orbital elements, orbital period, cross section, mass, and area-to-mass ratio.

Element	Unit	Symbol	LAGEOS II	Galileo FOC
Semi-major axis	[km]	a	12162.07	29599.8
Eccentricity	[–]	e	0.0138	0.0000
Inclination	[deg]	i	52.66	56.00
Orbital period	[s]	P	13348.2	50680.9
Cross section	[m^2]	A	0.2827	13.2100
Mass	[kg]	M	405.380	709.138
Area/Mass	[m^2/kg]	A/M	6.97500×10^{-4}	1.86283×10^{-2}

(ILRS) [29]. The first column provides the physical effect responsible of the perturbation, while the second column gives the mathematical expression used to compute the order-of-magnitude of the corresponding acceleration. Finally, the third column provides the main parameters affecting the knowledge of the perturbation. LAGEOS II can also be considered a point of reference, since the best and most sophisticated models for the NGPs have been developed for its linear and rotational dynamics [50,115–117].

In Table III are shown, for each of the considered satellites, the orbital elements used to estimate the accelerations of Tables I and II (in particular the semimajor axis) with other parameters, as the area-to-mass ratio, useful for the estimate of the accelerations produced by the main NGPs.

For the normalized gravity field coefficients, $\bar{C}_{\ell,m}$, those provided by the GGM05S model [118] from GRACE [119] data have been used. For the maximum degree, we considered $\ell = 12$, the truncation level (degree ℓ and order m) suggested by current IERS Conventions 2010 for the GNSS satellites [120] and the Earth's gravitational coefficient $GM_\oplus$ is still from IERS Conventions 2010. The main correction to the Newtonian equation of motion due to general relativity (GR) is also shown in Table I.

In the following, a few (but significant) considerations on the role of the NGPs on the Galileo satellites can be derived by the analysis of Table II together with previous considerations on their corresponding models.

(1) The obvious consideration is the role played by the value of the satellite's area-to-mass ratio. This immediately translates into a peak value for acceleration due to SRP of more than a factor of 40 greater for Galileo satellites than for LAGEOS II.
(2) A second aspect is related to the greater distance from the Earth, which in part (apparently) compensates for the larger A/M of the Galileo, as can be seen from the effects due to the albedo and infrared radiation pressure compared to those on LAGEOS II.
(3) The range of variability of the considered accelerations cover several orders of magnitude: three orders of magnitude in the case of the Galileo FOC satellites (from $\approx 10^{-7}$ m/s^2 down to $\approx 10^{-10}$ m/s^2), and about four orders of magnitude for LAGEOS II (from $\approx 10^{-9}$ m/s^2 down to $\approx 10^{-13}$ m/s^2).
(4) In the case of LAGEOS II several improved (and refined) models have been developed to account for the behavior of the perturbations down to a level of acceleration $\approx 10^{-12}$ m/s^2 [40,45,47,49,50,53,117,121]; conversely, in the case of the Galileo FOC current models account only down to about 10^{-10} m/s^2, but with several drawbacks.
(5) Because of the complex shape of the Galileo FOC and the additional fact that they are active satellites, also the uncertainties of the parameters that enter in their modeling are (in general) larger with respect to those of LAGEOS II (see next subsection).

Therefore, the overall modeling is worse in the case of the Galileo satellites with respect to LAGEOS-like satellites; this also explains why we used the term "apparently" in the point 2. above. Indeed, from all the literature available on GNSS satellites it is evident that a number of different NGPs are competing in the acceleration range between 10^{-9} m/s^2 and 10^{-10} m/s^2 [19,20,122]. This acceleration interval represents the granularity of the NGPs, within which it is difficult to clearly and univocally separate the various effects that make it up. Therefore, we can affirm that the actual "*noise level*" of the current NGPs models is around 10^{-10} m/s^2. This level of uncertainty can also be simply obtained from Table II considering the uncertainty of the main parameter that characterizes each perturbative acceleration. These aspects will be further discussed in the next subsection.

We finally conclude with a brief discussion on the use of the empirical terms, the outstanding example in the field of GNSS is represented by the so-called Y-bias, see Table II. We have already highlighted the positive role of empirical terms in absorbing unknown effects at the price, however, of losing the physical content of some perturbative effects. In the end, in the GNSS literature, it seems that the main objective is to reduce the POD residuals of these satellites by exploiting the modeling of the direct SRP, currently with a BW, and absorbing the other effects, as much as possible, through the *ad hoc* introduction of empirical terms, which however have the primary objective of absorbing the

unmodeled part of the SRP which is not taken into account by the BW model (see [20]).

This aspect is clearly expressed in the paper by [17]: "In our case, the interest is not to study the effects of SRP on the orbits, but rather to fit the measurements of the orbits (GPS tracking data) with a model capable of compensating the SRP acting on the satellites, which is assumed to be the major error source affecting the GPS satellite orbits. By doing this an improvement in the orbits themselves is also expected."

The last sentence, "*By doing this an improvement in the orbits themselves is also expected*," is in principle correct because, in the end, thanks to the empirical terms, it is possible to reduce the orbit residuals, and this is positive for Positioning, however, the sentence is questionable for other applications of GNSS satellites, such as for geophysics and fundamental physics.

As a methodological guideline, our interest is, contrary to that of [17], to understand the effects of the SRP on the orbital elements of navigation satellites and, in particular, for the Galileo ones. On these aspects, see the accompanying article [123], hereafter Paper II. For these reasons, we believe that a greater effort must be made in modeling the perturbative effects of nongravitational origin, in order to reduce their current limits. This will also help to establish the characteristics of an onboard accelerometer that can match, complement and overcome the performance of the models themselves within a POD.

A. NGPs intrinsic uncertainties

In this section, we will try to analyze the intrinsic precision of the models, without taking into account their precision/accuracy within an analysis based on the reduction of observational data, i.e., within a POD, with the consequent possible estimate of some parameters of the models themselves and/or of any empirical terms. We will limit this analysis to nongravitational perturbations. In fact, in the case of gravitational perturbations, the accelerations linked to the uncertainties of the various coefficients that characterize them—starting from that of the terrestrial quadrupole which produces the greatest acceleration, approximately 8×10^{-12} m/s^2—are much smaller than those attributable, for example, to thermal effects as indicated in Table II.

Based on the results obtained for the order of magnitude of the accelerations estimated for the various NGPs acting on a Galileo satellite, see Table II and the relative discussion, we will limit our analysis on the precision of the models to effects with accelerations $\geq 10^{-10}$ m/s^2. Of course, the two most important effects to be considered are the perturbations due to the direct and indirect SRP effects (i.e., the albedo).

In Table IV are shown the estimates, in order of magnitude, of the precision for some of the models of Table II. In column 2, the main parameters limiting the precision of the perturbative effects of column 1 are highlighted. Column 3 provides an estimate of the relative uncertainty of said parameters. This is based on the knowledge that we currently have of the parameters that characterize the models or that we will be able to achieve in the case of a box-wing model that is more performing (i.e a R-BW) than the current ones based on the knowledge of the Galileo FOC metadata (i.e., S-BW).

The relative uncertainties allow us to rescale the amplitude of the accelerations in Table II and estimate their precision for the effects considered and for each satellite: LAGEOS II in column 4 and a Galileo FOC, modeled with a S-BW in column 5 and with a R-BW in column 6. As for the relative error, when several parameters, not correlated with each other, contribute to its estimate, the error is estimated on the basis of their quadratic sum, that is in a root-sum-squared fashion. In general, in a measurement process, relative error is an indication of measurement accuracy only in the absence of systematic errors. When there are systematic errors, relative error is only an indication of the precision of a measurement and not its accuracy.

In the current simplified context of model error analysis, we will not consider the actual accuracy of models, in the

TABLE IV. Intrinsic uncertainties of the models and corresponding uncertainties in acceleration. The uncertainties highlighted in column 3 were estimated through the quadratic sum of the errors of the parameters reported in column 2. The three values of this uncertainty refer, respectively, to LAGEOS II, to a Galileo approximated by a simplified box-wing (S-BW) model and to a Galileo approximated by a reliable box-wing (R-BW) model. Column 5 provides an estimate of the error in acceleration in the case of a Galileo FOC modeled with a S-BW model based on current Galileo metadata information. Conversely, column 6 provides an estimate of the error in the hypothesis of a Galileo FOC modeled with a R-BW model constructed with more detailed information than that of the Galileo metadata. A R-BW model must be considered a preliminary FEM.

Physical effect	Parameter	Relative uncertainty	LAGEOS II	S-BW	R-BW
Direct SRP	$C_R, \frac{A}{M}, \Phi_\odot$, Optical coefficients	0.02/0.30/0.05	6.4×10^{-11}	3.0×10^{-8}	5.0×10^{-9}
Earth's albedo	$\frac{A}{M}, \Phi_\odot, A_\oplus$, Optical coefficients	0.30/0.43/0.30	3.9×10^{-11}	3.0×10^{-10}	2.1×10^{-10}
Earth's infrared radiation	$\frac{A}{M}, \Phi_{\mathrm{IR}}$, Optical coefficients	0.1/0.1/0.1	1.5×10^{-11}	1.1×10^{-10}	1.1×10^{-10}
Power from antennas	P, M, ξ	/0.06/0.02		7.2×10^{-11}	2.4×10^{-11}
Thermal effect solar panels	$\frac{A}{M}, \epsilon, T$	/0.06/0.03		1.1×10^{-11}	5.7×10^{-12}
Y-bias	Y_0	/0.086/0.043		6.0×10^{-11}	3.0×10^{-11}

sense of estimating their systematic errors. This aspect will be addressed, as far as possible, in the context of a precise determination of the orbit in a future work.

The following preliminary considerations can be drawn from the analysis of Table IV:

(1) It is interesting to note that in the case of the Galileos, when the noise threshold of the NGPs ($\simeq 10^{-10}$ m/s^2) and the *a priori* errors of the model parameters are considered, the perturbations to be effectively taken into account are restricted to the first three in magnitude: direct SRP, Earth's albedo and infrared radiation.
(2) However, only the uncertainty of the SRP acceleration is well above the "*noise level*" of the NGPs that characterize the Galileo satellites, whereas the acceleration uncertainty of both the terrestrial albedo and infrared radiation pressure falls within this "*noise level*."
(3) This means that the acceleration uncertainties in the models of albedo and infrared radiation are of the order of the perturbative effects produced by other (smaller) nonconservative forces, such as thermal effects.
(4) Therefore, several different nongravitational forces combine to create a sort of limbo within which, up to now, it is not possible to clearly separate the different perturbative effects in order to improve the global dynamic model of the orbit of the Galileo satellites, and of GNNS satellites in general.
(5) A better understanding of thermal effects and their inclusion in the dynamic model is yet to come; an indispensable prerequisite in this direction remains a significant improvement of the overall model, solar and terrestrial, for the effects deriving from the radiation pressure.
(6) On the contrary, in the case of LAGEOS II, the acceleration uncertainties are between 1 and 2 orders of magnitude greater than the noise level of its dynamic model for NGPs, consequently their effects can be well distinguished from those of other smaller perturbations.
(7) A step toward an R-BW model, midway between an S-BW model and an FEM, will probably only allow for model improvement for direct SRP, but improvements in albedo and terrestrial infrared radiation will likely not be significant.

As previously highlighted, here we analyzed the inherent precision of NGPs models and not their posterior accuracy once included in the POD process. Of course, during the POD, improvements are present thanks to the estimation and adjustment of the model parameters.

The results we have derived are obviously a function of the overall relative error we have assumed for each of the models considered in Table IV. The relative uncertainties indicated in the table are based on estimates made for the respective parameters in independent analyzes, and obviously cannot be considered completely reliable, also thanks to the currently scarce information on the characteristics of the Galileo FOC satellites. Nevertheless, even assuming a factor of 2 or 3 of discrepancy with respect to more truthful values, the quality and substance of the previous arguments do not fail.

A further aspect to consider when discussing the results shown in Table IV is related to the spectral content of the perturbations considered. In fact, in the case of perturbations characterized by a different spectral content, these are in principle more easily separable even if of comparable amplitudes. It is also important to underline that, once a given perturbation is fixed, the spectrum associated with it depends precisely on the goodness of the model used to include it in the dynamic model of the orbit: the spectrum obtained with a box-wing model will be richer in details than the one which is obtained with a cannon ball, but less detailed than the spectrum that can be obtained with a FEM for the spacecraft. For the details of the spectral content we obtained with our box-wing model we refer to Paper II.

Finally, an aspect to consider concerns the difference between periodic perturbations and constant or slowly variable perturbations over time. The latter can be absorbed by an empirical term that can make up for the lack of an adequate model. This is the case of the Y-bias acceleration, or the case of the acceleration due to the antennas, which is mainly directed radially outward from the Earth. Conversely, in the case of periodic effects, the advantage of a reliable model (or of an accelerometer) is indisputable. This is the case of the direct solar radiation pressure. In this case, see Table IV, we can see the clear advantage of a reliable model in determining more precisely the amplitude of periodic effects, at orbital frequency and its higher multiples [124].

V. TOWARDS THE FEM: 3D-CAD AND PRELIMINARY BOX-WING

As previously anticipated, the Metadata provided by ESA on the characteristics of Galileo satellites, although in general they are useful and rich in multiple information, are not sufficiently detailed for the construction of a complex model for the structure of a Galileo FOC type satellite, as in the case of a FEM.

Tables V and VI, adapted from ESA Metadata, show the available information regarding the dimensions of the box

TABLE V. Dimensions and surface areas of the box of Galileo FOC satellites from ESA metadata.

Dimensions [m]		Surface areas [m^2]	
ΔX	2.530	$\pm X$ panel	1.320
ΔY	1.200	$\pm Y$ panel	2.783
ΔZ	1.100	$\pm Z$ panel	3.036

TABLE VI. Surfaces of the satellite with their (approximated) materials, corresponding area and optical coefficients from ESA metadata. The physical meaning of these optical coefficients was introduced in the previous Sec. III B 4 and should be understood as average values for the coefficients of the materials in the visible part of the electromagnetic spectrum.

Surface		Material	Area m^2	α	ρ	δ
Box	+X	A	0.440	0.93	0.00	0.07
		C	0.880	0.08	0.73	0.19
	−X	A	1.320	0.93	0.00	0.07
	+Y	A	1.129	0.93	0.00	0.07
		C	1.654	0.08	0.73	0.19
	−Y	A	1.244	0.93	0.00	0.07
		C	1.539	0.08	0.73	0.19
	+Z	A	1.053	0.93	0.00	0.07
		B	1.969	0.57	0.22	0.21
	−Z	A	2.077	0.93	0.00	0.07
		C	0.959	0.08	0.73	0.19
Wing	+SA	E	3.880	0.92	0.08	0.00
		D	1.530	0.90	0.10	0.00
	−SA	E	3.880	0.92	0.08	0.00
		D	1.530	0.90	0.10	0.00

spacecraft and the average optical coefficients for the box panels and for the solar array (SA) of the Wings. The dimensions are provided with respect to the mechanical reference frame (MRF) of the spacecraft, see Fig. 1, while the complex elements located on the surfaces of the all spacecraft, especially of the box, are approximated by a few materials.

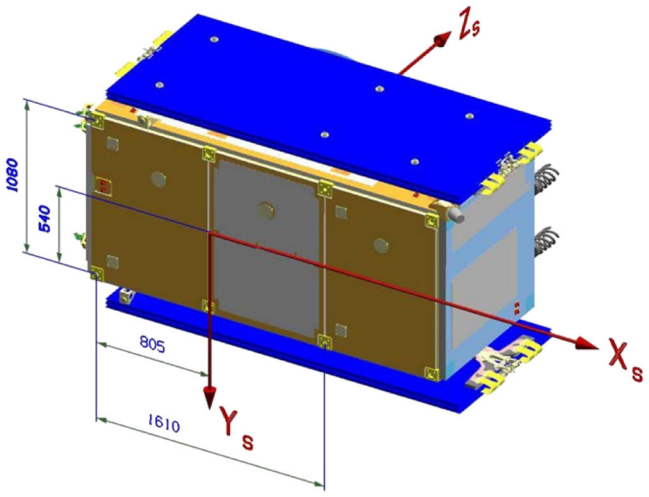

FIG. 1. Galileo FOC spacecraft: the mechanical reference frame. The MRF s aligned with the main body axes and originates in the separation plane of dispenser and satellite in the exact middle of the four I/F point center lines. The $+Z_s$-axis is normal to the separation plane and points toward the L-band navigation antenna. The $+X_s$-axis is normal to the clock panel and points toward the clock panel. The $+Y_s$-axis completes the right-handed orthogonal system. Courtesy of ESA from Galileo metadata.

As we can see from Table VI, five different materials (letters A–E) have been introduced as a very rough approximation of the real spacecraft. This is evident if we consider the surface $+Z$, that is, the one facing the Earth. This surface in the Metadata was considered to consist of only two materials, A and B, whose combined characteristics are not comparable with those of the real components of the surface. In fact, the real surface (see Fig. 2) is equipped with a set of antennas (e.g. L-band SAR and C-band) [125], corner cube retroreflectors (CCR) and Earth sensors, just to mark the most evident differences, which have very different optical characteristics from each other and also compared to those of the same metadata.

However, as shown in Fig. 3 for the flight version of the spacecraft, both the L-band antenna and the exagonal surface occupied by the SAR antennas are covered by a Mylar sheet coated with Silver and Beryllium. This means that for these elements, the mylar optical properties must be considered in the modeling process. Therefore, considering the properties of the mylar and not those of the L-band antenna, represents one of the necessary steps toward the construction of a satellite model more relevant to reality

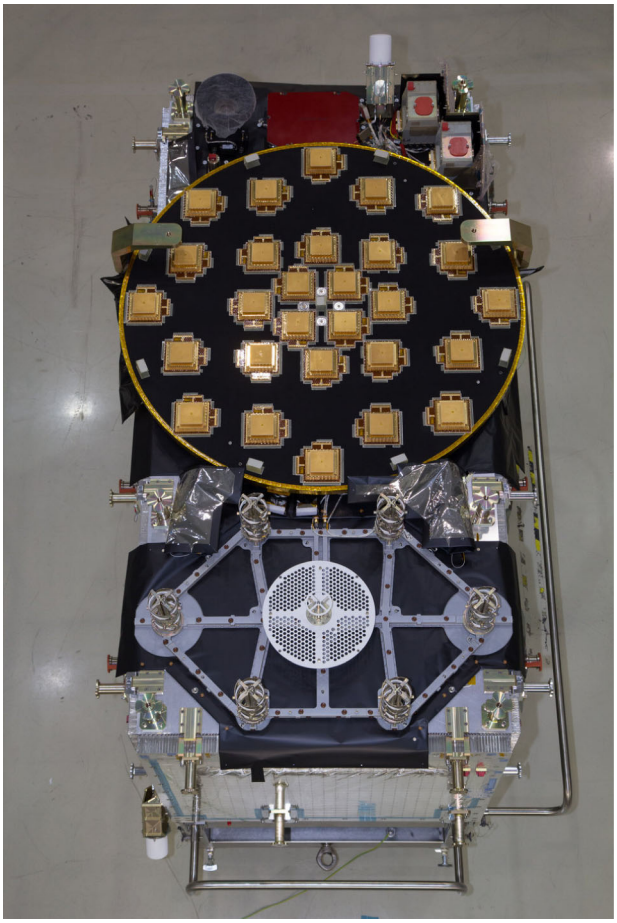

FIG. 2. Galileo FOC spacecraft: photo of the $+Z$ panel. Courtesy of ESA.

FIG. 3. Galileo FOC spacecraft: photo of four satellites at OHB in Bremen. Courtesy of ESA.

than a simple box-wing based on Galileo metadata. In the case of the SAR antennas, three different materials have to be considered: (i) the mentioned mylar sheet for the exagonal plate, (ii) Aluminium (probably anodized) for the six radiating elements (the elicoidal antennas), and (iii) a white paint for the circular plate (i.e., the subreflector ground plate).

It should be noted that the nonsmooth surface of the mylar will complicate the correct application of the ray-tracing technique for these elements, giving for example a partly random character to the specular reflection.

Therefore, if ESA (or OHB, which built the satellites) does not release further updates of the optical properties for the different surface elements in the future, and with sufficient detail to build a FEM (or at least a R-BW model), it will be necessary to proceed with *ad hoc* hypotheses, the most plausible from the physical point of view, to fix the values for the physical properties of the various materials. In this case, the results of the PODs will give us a rough indication (necessarily more qualitative than quantitative) on the validity of our *a priori* hypotheses, for example on the basis of the statistic and distribution of the post-fit residuals obtained.

In the following sections, we present the 3D model and a box-wing model for the spacecraft that we built for the forthcoming activities of G4S_2.0.

A. 3D-CAD model with SolidWorks

Since the information contained on the metadata of the Galileo satellites is very scarce, all the dimensions necessary to build a 3D model of the satellite have been obtained indirectly, such as the distances between the different elements of the surfaces and their location on the same, through the numerous photographs of the Galileo FOC satellites available on the web.

In fact, we reconstructed the size and position of the different parts of the satellite based on the large amount of photos, taken from many points of view, representing the satellite during assembly and ground tests by ESA. A very powerful tool for this process was the SketchUp program ([126]).

Using this program we have first drawn a parallelepiped having the dimensions reported in the Galileo metadata for the box, see Table V. Then, many photos representing the different parts of the satellite have been matched to this drawing. The program allows to modify the representation of the 3D model drawn in it, changing the point of view and the focal length. Consequently, these parameters have been modified trying to perfectly superimpose the drawing on the photo used as background.

The program also allows you to "glue" the corresponding parts of the photo to the sides of the 3D solid. After pairing, if you choose a different perspective to view the 3D box, the part of the photo changes along with the side it is pasted on. By choosing the most convenient perspective, using the program's "measure" tool, it is possible to obtain the positions of the different components on each face, as said. Of course, the operation is much less affected by error the more the photo used is taken from a direction normal to the surface. Finally, the different measurements obtained with this procedure were used to draw a 3D model in a CAD (Computer Aided Design): SolidWorks ([127]) was used [128].

This is shown in Figs. 4 and 5 for our current 3D-CAD model of the Galileo FOC spacecraft. From these figures it is possible to detect the high degree of detail of the surfaces achieved in our model, as can be seen from their comparison with the photo of the satellite shown in Fig. 2.

Naturally, to proceed with the application of ray-tracing, the different surfaces and the different elements of the 3D model must be discretized to a level of detail suitable for

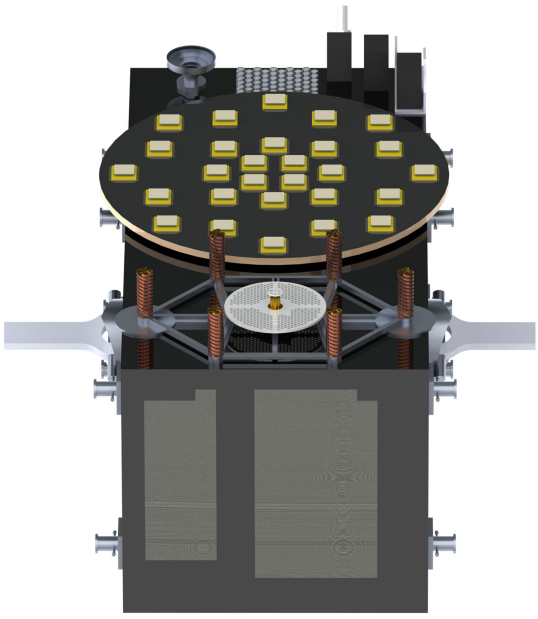

FIG. 4. 3D-CAD model of a Galileo FOC spacecraft. The $+Z$ and $+X$ surfaces are shown.

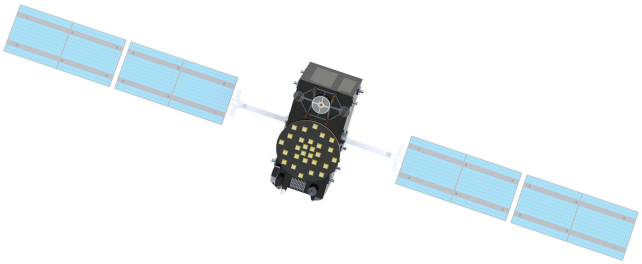

FIG. 5. 3D-CAD model of a Galileo FOC spacecraft. The $+Z$ and $+X$ surfaces are shown with the solar panels.

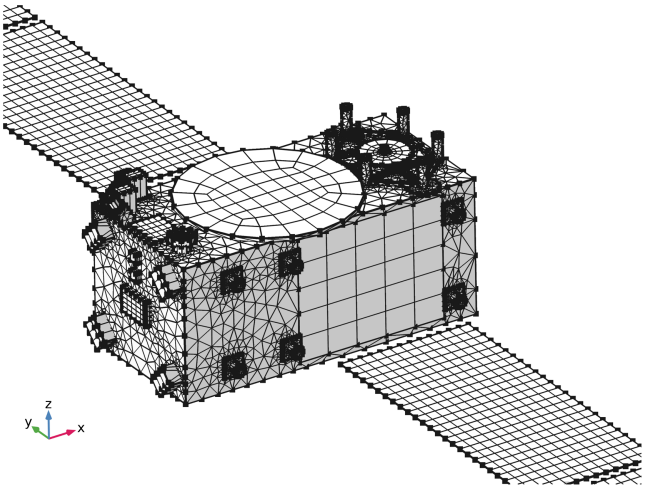

FIG. 6. A very preliminary partial mesh of the 3D-CAD model of a Galileo FOC spacecraft. The $+Z$, $-X$ and $-Y$ surfaces are shown with part of the solar panels.

them by means of an appropriate mesh. In Fig. 6, it is shown a preliminary rough example of mesh produced with COMSOL [129].

B. S-BW model and COMSOL

In Sec. III A we underlined the difficulties that can be encountered to fully characterize a FEM of the Galileo FOC spacecraft from the physical point of view. In case these difficulties will be not overcome, due to lack of necessary information, we will focus on developing a superior box-wing which we have already called in Sec. III B 5 as a reliable box-wing (R-BW) model. This R-BW model will have to be characterized by the greatest possible number of information for the different surfaces and the different elements that compose them.

A ray tracing algorithm is being developed in MATLAB code and while we are currently finalizing the code in MATLAB to test them on the FEM or on the R-BW of the Galileo FOC satellites, we have proceeded with the start of a preliminary activity on our box-wing model of the satellite—the S-BW model built with ESA metadata—embedded within the COMSOL MultiPhysics [129] tools.

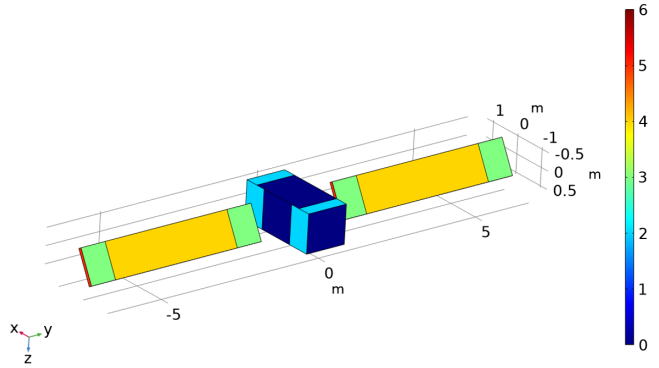

FIG. 7. COMSOL representation of the S-BW model for a Galileo FOC spacecraft based on ESA Metadata. The different colors reflect the materials in Table VI with the corresponding optical coefficients.

Figure 7 shows the COMSOL version of the S-BW model used in our simulations. The box-wing is drawn respecting the dimensions and areas described in Table V, while the colors correspond to the materials (and corresponding areas) described in Table VI. The reference system corresponds to the MRF previously introduced in Fig. 1.

The simulation was parameterized with respect to an angle ψ ranging between 0° and 180°, which is defined as the angle of the +X vector referred to the box around +Y, from its initial position −Z (corresponding to $\psi = 0°$) to its final position +Z (corresponding to $\psi = 180°$). The unit vector $\hat{\mathbf{e}}_{\mathbf{D}}$, that identifies the direction of the Sun, also rotates following ψ. Solar panels have always been considered orthogonal to the direction of the Sun and therefore not rotating with the box of the satellite.

The *view factors* were calculated by COMSOL using the physics of its "surface-to-surface radiation" module [130]. Not using at the moment the ray-tracing technique of COMSOL, that of the calculation of the *view factors* is an expedient to determine the quantity of solar radiation that radiates each surface of the satellite in order to be able to determine the corresponding acceleration according to Eq. (5). Figure 8 shows the values of the *view factors* (color bar) when $\psi = 60°$.

Once the accelerations acting on each face of the S-BW have been calculated, these are projected into the body frame of the spacecraft identified by the MRF. These accelerations, and the corresponding absolute value, are plotted in Fig. 9 as a function of ψ. Obviously the acceleration along the Y-axis is always zero in this ideal situation (i.e., with the solar panels always orthogonal to the Sun direction) and furthermore the acceleration due to the wings is constant.

We then proceeded to compare the solution for the accelerations produced by direct solar radiation using the COMSOL model for the S-BW with a numerical solution obtained with a specially developed MATLAB numerical

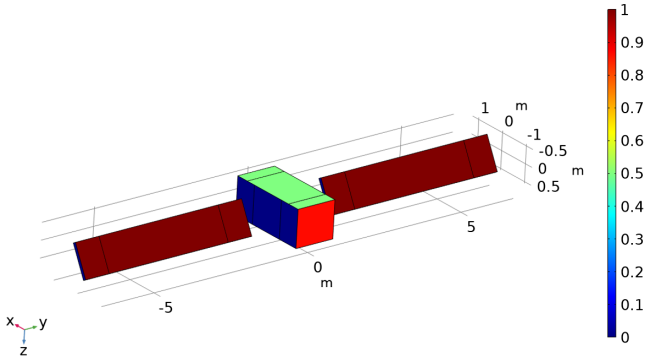

FIG. 8. View factors for the S-BW model in COMSOL for $\psi = 60°$. For clarity, when $\psi = 0°$ the solar rays are orthogonal to the $-Z$ face of the satellite, when $\psi = 90°$ the solar rays are orthogonal to the $-X$ face, and finally when $\psi = 180°$ the solar rays are orthogonal to the $+Z$ face.

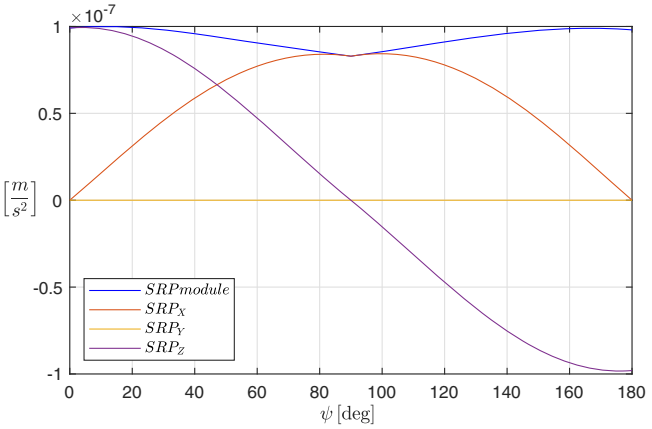

FIG. 9. Direct SRP acceleration in the body frame identified by the MRF. The components and the absolute value (blue line) of the acceleration due to the Sun radiation pressure are plotted as a function of the rotating angle ψ.

code ([131]). As already specified, this second model and the corresponding solutions are described in detail in Paper II in the case of the direct SRP. In particular we:

(1) Verified the consistency of the reference systems used.
(2) Verified the consistency of the results on the single surfaces of the satellite.
(3) Compared the results over a 500 days simulation.

Figure 10 shows the comparison for the module of the acceleration produced by the SRP acting on the S-BW obtained with the COMSOL model and with the MATLAB numerical code. Since in the model developed in MATLAB the accelerations are calculated as a function of time, first of all the COMSOL vs angle solution was transformed into a COMSOL vs time solution. Therefore, a time vector has been constructed which interpolates the COMSOL solution vs angle for each angle vs time. For simplicity, in this test the Earth-Sun distance was considered fixed at 1

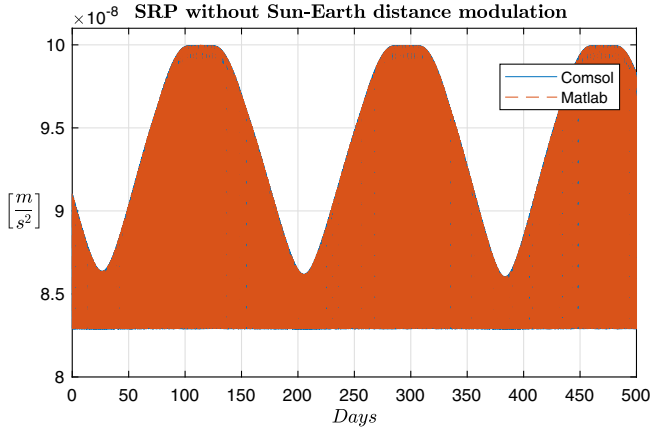

FIG. 10. Absolute value of the direct SRP acceleration on the S-BW model obtained with COMSOL (blue line), as a function of time, compared to the same acceleration obtained with the S-BW model implemented with MATLAB (brown line).

astronomical unit, as it does not affect the quality of the comparison.

As can be seen, the two solutions are practically coincident. The only significant difference lies with the different attitude law of the spacecraft in the two cases. In the case of COMSOL, a nominal attitude was always assumed with the surface of the solar panels orthogonal to the solar radiation. In the case of the numerical code, the attitude variation of the satellite during the eclipses season was taken into account according to the attitude variation described in the ESA Metadata. This is shown in Fig. 11, where the difference between the two accelerations is plotted.

The three minimum in acceleration, lasting about 10 days each, characterize the eclipse season—that is, when the Sun is relatively low on the satellite's orbital plane—with a periodicity of about 175 days. The residual acceleration that can be seen in the figure, which is characterized by an

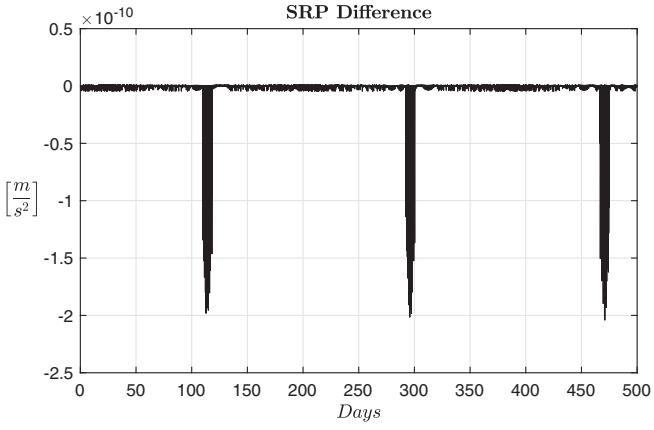

FIG. 11. Difference in the asolute value of the direct SRP acceleration obtained with the MATLAB model with the corresponding acceleration obtained with COMSOL.

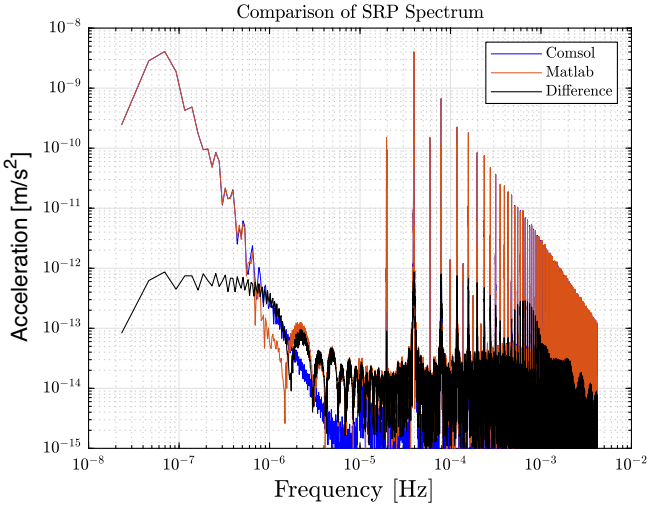

FIG. 12. Fast Fourier transform of the absolute value of the SRP as obtained with COMSOL (blue) and with the numerical code (orange) and of their difference (black).

average value of about -5×10^{-14} m/s^2 and a peak-to-peak variation of about 5×10^{-12} m/s^2, is actually a numerical artifact of the current integration process in MATLAB. In fact, it does not in itself constitute a problem: on the one hand it can be canceled by decreasing the integration step in the model developed in MATLAB (currently 120 s), while on the other hand we are interested in reaching a level of precision in the modeling of the nongravitational accelerations down to the order of 10^{-10} m/s^2, as the one reached during the eclipse season, i.e., two order-of-magnitude larger than the peak-to-peak variation in Fig. 11. Figure 12 provides the representation of Figs. 10 and 11 in the frequency domain. As can be seen, the lines at the orbital frequency of the satellite ($f_{\rm orb} \simeq 1.97 \times 10^{-5}$ Hz) and at its higher integer multiples are clearly visible both in the case of the COMSOL model and in the numerical one obtained with MATLAB. In the case of the spectrum of the difference between the two models, the amplitudes of the lines are of the order of $\approx 10^{-12}$ m/s^2.

The next steps in the use of COMSOL concern the implementation of the rotation of the satellite around the yaw axis, i.e., around the Earth-satellite radial direction and a first application of the MATLAB ray-tracing algorithms to a simplified 3D model of the spacecraft with respect to the one presented in Sec. V A.

VI. CONCLUSIONS AND RECOMMENDATIONS

In this work we introduced some of the activities currently in progress at IAPS/INAF within the G4S_2.0 project. These activities focus on the study of nonconservative forces on the Galileo FOC satellites and the consequent development of an appropriate model of the real satellite in order to account for their perturbative effects. In this regard, the main challenge is to significantly improve, compared to the state of the art, the modeling of the orbital effects related to the direct solar radiation pressure, indeed the largest nongravitational perturbation on GNSS satellites. This is motivated by the fact, as already highlighted above, that some of the ambitious goals of G4S_2.0—such as an improvement in the accuracy of the gravitational redshift measurement or the measurement of relativistic precessions on the orbits of the GSAT-0201 and GSAT-0202 satellites—require an improvement of the dynamic model of the orbits of the Galileo FOC satellites, starting with the model of perturbations of nongravitational origin.

In order to fully carry out this task, the state of the art was then evaluated (see Secs. II and III) with regard to the main models developed so far in the literature to take into account the perturbative effects produced by the direct solar radiation pressure and by other (much smaller) nonconservative forces that act on the Galileo FOC satellites and on the GNSS satellites in general. This allowed us to feature the types and peculiarities of the different models, highlighting their advantages and disadvantages, as well as their actual degree of implementation in the orbit determination softwares. For example, the models based on a satellite FEM, although developed by several authors in the literature, do not seem to be used by the different GNSS analysis centers, generally preferring a simple box-wing model with the concomitant estimate of a certain number of empirical accelerations. This is probably linked both to the difficulty of including the FEM of the spacecraft in the PODs processes with the consequent application of the ray-tracing technique to it, and to an actual lack of an accurate knowledge of the "fine structure" of the satellites, starting with their optical properties and their consequent evolution (say degradation) with the passage of time. As described in the previous sections, we are interested in developing a *superior* model of the satellite, possibly a model that comes as close as possible to a FEM, to be used in our PODs in the field of fundamental physics.

A significant aspect, we believe, of the work carried out in this first phase, was to quantify not only the orders of magnitude of the various nongravitational perturbations involved, an aspect already addressed in the literature but probably not with the extension and in-depth analysis we presented, but also to critically evaluate the intrinsic uncertainties of the current models and their possible improvement with more performing models (see Sec. IV). This has allowed us to establish that the current *intrinsic noise level* of the nongravitational accelerations that the models provide, currently in the $10^{-9} \div 10^{-10}$ m/s^2 range, may be reduced in the future down to 10^{-10} m/s^2 only if a great effort at the satellite knowledge level will be done by the space agencies and the industries in charge of the spacecraft construction and assembly, but it is unlikely that it will be reduced further. We therefore think that it is

fundamental for the new future constellations of GNSS satellites that the various space agencies involve the industry in a series of ground tests to finely characterize all the elements and surfaces of the satellites, in order to define all the useful physical properties to the development of new perturbative models for accelerations of nongravitational origin. Of course, once all this technical information has been determined, it will necessarily need to be shared with the scientific community.

Naturally, and this has been pointed out previously, here we are considering the intrinsic precision, *per se*, of the models, and not that which is obtained *a posteriori* thanks to the orbital determination process with the concomitant possible estimation of some of the parameters that characterize a certain perturbative model. For example, a model would be very useful for the knowledge of the temperature distribution on the surface of the satellite and inside it, in the two extreme cases in which the satellite is fully illuminated by the Sun and in the case of eclipses. In this case, the characterization of the thermal inertia of the different elements is of primary importance. In this regard, it was also underlined how an accelerometer, with appropriate sensitivity and measurement band, can provide a qualitative leap in this context thanks to the direct measurement of nongravitational accelerations and the process of their integration. This is in fact one of the objectives of the G4S_2.0 project, namely the development of an accelerometer for a future generation of Galileo satellites, the readings of which would in any case complement the predictions provided by the models without replacing them.

In Sec. V, we introduced the two models we developed so far the Galileo FOC spacecraft. The first is a 3D model of the satellite. As explained in Secs. III and V A, the final purpose is to best characterize the different elements of the satellite to create an appropriate mesh of the satellite and apply the ray-tracing technique on top of it. If this is successful, we will have a FEM of a Galileo FOC which will allow us first of all to greatly improve the modeling of the solar radiation pressure effects. In fact, as has been explained, the construction of a 3D-CAD of the satellite is the main prerequisite for the implementation of a satellite FEM. The most difficult part then lies in the detailed knowledge of the physical properties for the different elements and, finally, in the implementation of an optimal ray-tracing technique. These aspects will be addressed in the project's future activities.

The second satellite model we have built is a simplified box-wing (S-BW). This provides us with a basic model on which to evaluate future improvements on the satellite's model (i.e., toward the FEM) as our knowledge on its intrinsic physical characteristics (optical, thermal, etc.) increases. The first applications of the S-BW are described in the paper accompanying the present in this same issue. We will use, as one of the possible indicators to evaluate the goodness of our more detailed satellite models, the results of the PODs that we will obtain with the s/w GEODYN II [132], evaluating the range residuals (with their statistics) but also the orbital residuals [133] of the considered satellites. An important further application of the box-wing model is its use within COMSOL as a first experimental test bed for ray-tracing applications. The preliminary applications of the S-BW in this perspective have been described in Sec. V B, and constitute a sort of "*calibration*" of the S-BW in COMSOL for the continuation of these activities.

Finally, an aspect to be reiterated further, directly linked to what we have defined as the *intrinsic noise level* of the nongravitational accelerations, concerns the perturbative effects of thermal origin (Secs. II and IV). These can be taken into due consideration only when the perturbative effects produced by the pressure of the solar radiation (both direct and indirect) will reach a knowledge, in their main spectral components, at an acceleration level of the order of a few 10^{-10} m/s^2, however a very difficult task to accomplish.

Returning to fundamental physics measurements, at the current state of the development of G4S_2.0 activities, it is not possible to give a reliable answer on what the requirements of the NGPs models should be, for example, on the measurement of the relativistic Schwarzschild precession or on that of the gravitational redshift to obtain results comparable (or superior) to those reported in the literature on such tests of gravitation [7,8,33,34]. Meanwhile, as underlined in Sec. IV A, the final precision of the models must be evaluated only when they are completely used in the POD of the satellites for the reduction of the tracking data, whether laser or microwave. This very important aspect will be the subject of our future investigations, as was done in the past in the case of the LAGEOS and LAGEOS II geodetic satellites. In the case of the previous measurements on the gravitational redshift with the Galileo satellites in elliptical orbit, no information emerges from the literature regarding this aspect.

Of course, a general improvement in POD, thanks to better and more reliable models than the state of the art, will produce an improvement in fundamental physics measurements, but it is not certain that this improvement will be equally distributed among all the different types of measurements to be performed. For example, if the dynamical model is unable to prevent long-term effects in some orbital elements such as the pericenter, which constitutes the main observable for measuring the Schwarzschild precession, this will certainly impact this measure, but will in general be negligible in the estimation of the clock-bias and consequently in the measurement of the gravitational redshift.

ACKNOWLEDGMENTS

This work is part of the G4S_2.0 project, developed under the auspices of the Italian Space Agency (ASI) within the frame of the Bando Premiale CI-COT-2018-085, under the Accordo Attuativo No. 2021-14-HH.0, with co-participation of the Italian Institute for Astrophysics (INAF) and the Politecnico di Torino (POLITO).

[1] F. Vespe, D. Lucchesi, A. Tartaglia, G. Delle Monache, R. Peron, E. Rosciano, F. Santoli, and M. Visco, GALILEO for Science project (G4S): An opportunity to perform new measurements in fundamental physics, in *Proceedings of the 6th International Colloquium on Scientific and Fundamental Aspects of GNSS/Galileo* (European Space Agency, Valencia, Spain, 2017).

[2] F. Vespe, GALILEO for Science project (G4S): Eccentric GALILEO satellites for general relativistic investigations, in *Proceedings of the 42nd COSPAR Scientific Assembly* (COSPAR, Pasadena, 2018), Vol. 42, p. H0.5-3-18.

[3] D. Lucchesi, G. Delle Monache, R. Peron, E. Rosciano, M. L. Ruggiero, F. Santoli, A. Tartaglia, M. Visco, and F. Vespe, The Galileo for Science (G4S) project: Fundamental physics and space geodesy by the orbit analysis of the Galileo satellites DORESA and MILENA, in *Proceedings of the EGU General Assembly Conference Abstracts*, EGU General Assembly Conference Abstracts (EGU, Vienna, 2018), p. 15185.

[4] M. L. Ruggiero, A. Tartaglia, D. Lucchesi, G. Delle Monache, R. Peron, E. Rosciano, F. Santoli, F. Vespe, and M. Visco, Fully relativistic positioning for the Galileo for Science (G4S) project, in *Proceedings of the EGU General Assembly Conference Abstracts*, EGU General Assembly Conference Abstracts (EGU, Vienna, 2018), p. 12644.

[5] F. Sapio, D. M. Lucchesi, M. Visco, S. Benedetti, E. Fiorenza, C. Lefevre, M. Lucente, C. Magnafico, R. Peron, and F. Santoli, The Galileo for Science (G4S_2.0) project: Fundamental Physics experiments with Galileo satellites DORESA and MILENA, Nuovo Cimento Soc. Ital. Fis. **45C**, 1 (2022).

[6] A. Di Marco, F. Sapio, M. Cinelli, E. Fiorenza, C. Lefevre, P. Loffredo, D. M. Lucchesi, M. Lucente, C. Magnafico, R. Peron, F. Santoli, and M. Visco, The Galileo for Science (G4S_2.0) project: Measurement of the gravitational redshift with Galileo satellites DORESA and MILENA, Nuovo Cimento Soc. Ital. Fis. **45C**, 1 (2023).

[7] S. Herrmann, F. Finke, M. Lülf, O. Kichakova, D. Puetzfeld, D. Knickmann, M. List, B. Rievers, G. Giorgi, C. Günther, H. Dittus, R. Prieto-Cerdeira, F. Dilssner, F. Gonzalez, E. Schönemann, J. Ventura-Traveset, and C. Lämmerzahl, Test of the gravitational redshift with Galileo satellites in an eccentric orbit, Phys. Rev. Lett. **121**, 231102 (2018).

[8] P. Delva, N. Puchades, E. Schönemann, F. Dilssner, C. Courde, S. Bertone, F. Gonzalez, A. Hees, C. Le Poncin-Lafitte, F. Meynadier, R. Prieto-Cerdeira, B. Sohet, J. Ventura-Traveset, and P. Wolf, Gravitational redshift test using eccentric Galileo satellites, Phys. Rev. Lett. **121**, 231101 (2018).

[9] R. F. C. Vessot and M. W. Levine, A test of the equivalence principle using a space-borne clock, Gen. Relativ. Gravit. **10**, 181 (1979).

[10] R. F. C. Vessot, M. W. Levine, E. M. Mattison, E. L. Blomberg, T. E. Hoffman, G. U. Nystrom, B. F. Farrel, R. Decher, P. B. Eby, C. R. Baugher, J. W. Watts, D. L. Teuber, and F. D. Wills, Test of relativistic gravitation with a space-borne hydrogen maser, Phys. Rev. Lett. **45**, 2081 (1980).

[11] V. Formichella, L. Galleani, G. Signorile, and I. Sesia, Time–frequency analysis of the Galileo satellite clocks: Looking for the J2 relativistic effect and other periodic variations, GPS Solution **25**, 56 (2021).

[12] J. Kouba, Testing of general relativity with two Galileo satellites in eccentric orbits, GPS Solution **25**, 139 (2021).

[13] A. Einstein, Die Grundlage der allgemeinen relativitätstheorie, Ann. Phys. **354**, 769 (1916), https://onlinelibrary.wiley.com/doi/epdf/10.1002/andp.19163540702.

[14] C. M. Will, *Theory and Experiment in Gravitational Physics* (Cambridge University Press, Cambridge, United Kingdom, 2018).

[15] M. Rothacher, GENESIS: GNSS/NAV science programme, in *GSAC: Galileo Science Advisory Committee, ESA PB NAV Workshop on CM22* (Javier Ventura Traveset, 2021).

[16] G. Beutler, E. Brockmann, W. Gurtner, U. Hugentobler, L. Mervart, M. Rothacher, and A. Verdun, Extended orbit modeling techniques at the CODE processing center of the international GPS service for geodynamics (IGS): Theory and initial results, Manuscripta Geod. **19**, 367 (1994).

[17] C. Rodriguez-Solano, U. Hugentobler, and P. Steigenberger, Adjustable box-wing model for solar radiation pressure impacting GPS satellites, Adv. Space Res. **49**, 1113 (2012).

[18] D. Arnold, M. Meindl, G. Beutler, R. Dach, S. Schaer, S. Lutz, L. Prange, K. Sośnica, L. Mervart, and A. Jäggi, CODE's new solar radiation pressure model for GNSS orbit determination, J. Geodes. **89**, 775 (2015).

[19] O. Montenbruck, P. Steigenberger, and U. Hugentobler, Enhanced solar radiation pressure modeling for Galileo satellites, J. Geodes. **89**, 283 (2015).

[20] G. Bury, K. Sośnica, R. Zajdel, and D. Strugarek, Toward the 1-cm Galileo orbits: Challenges in modeling of perturbing forces, J. Geodes. **94**, 16 (2020).

[21] F. L. Whipple and Z. Sekanina, Comet Encke–precession of the spin axis, nongravitational motion, and sublimation, Astron. J. **84**, 1894 (1979).

[22] W. M. Smart, John Couch ADAMS and the discovery of Neptune, Pop. Astron. **55**, 301 (1947).
[23] A. Milani, A. M. Nobili, and P. Farinella, *Non-Gravitational Perturbations and Satellite Geodesy* (Adam Hilger, Bristol, 1987).
[24] O. Montenbruck and E. Gill, *SatelliteOrbits—Models, Methods and Application* (Springer, Berlin, 2005).
[25] G. Beutler, *Methods of Celestial Mechanics. Vol. I: Physical, Mathematical, and Numerical Principles* (Springer, New York, 2005), ISBN 3-540-40749-9.
[26] G. Beutler, *Methods of Celestial Mechanics. Vol. II: Application to Planetary System Geodynamics and Satellite Geodesy* (Springer, New York, 2005), ISBN 3-540-40750-2.
[27] B. Hofmann-Wellenhof, H. Lichtenegger, and E. Wasle, *GNSS—Global Navigation Satellite Systems—GPS, GLONASS, Galileo, and more* (Springer, New York, 2008), ISBN 978-3-211-73012-6.
[28] P. Teunissen and O. Montenbruck, *Springer Handbook of Global Navigation Satellite Systems* (Springer, Cham, 2017), https://dx.doi.org/10.1007/978-3-319-42928-1.
[29] M. R. Pearlman, J. J. Degnan, and J. M. Bosworth, The international laser ranging service, Adv. Space Res. **30**, 135 (2002).
[30] S. C. Cohen and D. E. Smith, Lageos scientific results: Introduction, J. Geophys. Res. **90**, 9217 (1985).
[31] I. Ciufolini, D. Lucchesi, F. Vespe, and A. Mandiello, Measurement of dragging of inertial frames and gravitomagnetic field using laser-ranged satellites, Nuovo Cimento Soc. Ital. Fis. **109A**, 575 (1996).
[32] I. Ciufolini and E. C. Pavlis, A confirmation of the general relativistic prediction of the Lense-Thirring effect, Nature (London) **431**, 958 (2004).
[33] D. M. Lucchesi and R. Peron, Accurate measurement in the field of the Earth of the general-relativistic precession of the LAGEOS II pericenter and new constraints on non-Newtonian gravity, Phys. Rev. Lett. **105**, 231103 (2010).
[34] D. M. Lucchesi and R. Peron, LAGEOS II pericenter general relativistic precession (1993-2005): Error budget and constraints in gravitational physics, Phys. Rev. D **89**, 082002 (2014).
[35] D. Lucchesi, L. Anselmo, M. Bassan, C. Pardini, R. Peron, G. Pucacco, and M. Visco, Testing the gravitational interaction in the field of the Earth via satellite laser ranging and the Laser Ranged Satellites Experiment (LARASE), Classical Quantum Gravity **32**, 155012 (2015).
[36] D. M. Lucchesi, L. Anselmo, M. Bassan, C. Magnafico, C. Pardini, R. Peron, G. Pucacco, and M. Visco, General relativity measurements in the field of Earth with laser-ranged satellites: State of the art and perspectives, Universe **5**, 141 (2019).
[37] I. Ciufolini, A. Paolozzi, E. C. Pavlis, G. Sindoni, J. Ries, R. Matzner, R. Koenig, C. Paris, V. Gurzadyan, and R. Penrose, An improved test of the general relativistic effect of frame-dragging using the LARES and LAGEOS satellites, Eur. Phys. J. C **79**, 872 (2019).
[38] D. Lucchesi, M. Visco, R. Peron, M. Bassan, G. Pucacco, C. Pardini, L. Anselmo, and C. Magnafico, A 1% measurement of the gravitomagnetic field of the Earth with laser-tracked satellites, Universe **6**, 139 (2020).
[39] D. Vokrouhlicky, P. Farinella, and F. Mignard, Solar radiation pressure perturbations for Earth satellites. 1: A complete theory including penumbra transitions, Astron. Astrophys. **280**, 295 (1993), https://articles.adsabs.harvard.edu/pdf/1993A%26A...280..295V.
[40] D. P. Rubincam, On the secular decrease in the semimajor axis of LAGEOS's orbit, Celest. Mech. **26**, 361 (1982).
[41] G. Afonso, F. Barlier, F. Mignard, M. Carpino, and P. Farinella, Orbital effects of LAGEOS seasons and eclipses, Ann. Geophys. **7**, 501 (1989).
[42] P. Farinella, A. M. Nobili, F. Barlier, and F. Mignard, Effects of thermal thrust on the node and inclination of LAGEOS, Astron. Astrophys. **234**, 546 (1990), https://articles.adsabs.harvard.edu/pdf/1990A%26A...234..546F.
[43] R. Scharroo, K. F. Wakker, B. A. C. Ambrosius, and R. Noomen, On the along-track acceleration of the LAGEOS satellite, J. Geophys. Res. **96**, 729 (1991).
[44] V. J. Slabinski, A numerical solution for LAGEOS thermal thrust: The rapid-spin case, Celest. Mech. Dyn. Astron. **66**, 131 (1996).
[45] P. Farinella and D. Vokrouhlický, Thermal force effects on slowly rotating, spherical artificial satellites-I. Solar heating, Planet. Space Sci. **44**, 1551 (1996).
[46] D. P. Rubincam, D. G. Currie, and J. W. Robbins, LAGEOS I once-per-revolution force due to solar heating, J. Geophys. Res. **102**, 585 (1997).
[47] G. Métris, D. Vokrouhlický, J. C. Ries, and R. J. Eanes, Nongravitational effects and the LAGEOS eccentricity excitations, J. Geophys. Res. **102**, 2711 (1997).
[48] G. Métris, D. Vokrouhlický, J. C. Ries, and R. J. Eanes, LAGEOS spin axis and non-gravitational excitations of its orbit, Adv. Space Res. **23**, 721 (1999).
[49] D. M. Lucchesi, Reassessment of the error modelling of non-gravitational perturbations on LAGEOS II and their impact in the lense-thirring derivation-Part II, Planet. Space Sci. **50**, 1067 (2002).
[50] J. I. Andrés de la Fuente, Enhanced modelling of LAGEOS non-gravitational perturbations, Ph.D. thesis, Delft University Press, Sieca Repro, 2007.
[51] D. P. Rubincam, P. Knocke, V. R. Taylor, and S. Blackwell, Earth anisotropic reflection and the orbit of LAGEOS, J. Geophys. Res. **92**, 11662 (1987).
[52] D. M. Lucchesi, The asymmetric reflectivity effect on the LAGEOS satellites and the germanium retroreflectors, Geophys. Res. Lett. **30**, 1957 (2003).
[53] D. M. Lucchesi, LAGEOS satellites germanium cube-corner-retroreflectors and the asymmetric reflectivity effect, Celest. Mech. Dyn. Astron. **88**, 269 (2004).
[54] H. P. Robertson, Dynamical effects of radiation in the solar system, Mon. Not. R. Astron. Soc. **97**, 423 (1937).
[55] I. I. Shapiro, The prediction of satellite orbits, in *Dynamics of Satellites / Dynamique des Satellites*, edited by M. Roy (Springer Berlin Heidelberg, Berlin, Heidelberg, 1963), pp. 257–312.
[56] R. R. Allan, Resonance effects due to the longitude dependence of the gravitational field of a rotating primary, Planet. Space Sci. **15**, 53 (1967).
[57] D. Vokrouhlicky, P. Farinella, and F. Mignard, Solar radiation pressure perturbations for Earth satellites. III. Global atmospheric phenomena and the Albedo effect,

Astron. Astrophys. **290**, 324 (1994), https://articles.adsabs.harvard.edu/pdf/1994A%26A...290..324V.
[58] L. Sehnal, Effects of the terrestrial infrared radiation pressure on the motion of an artificial satellite, Celest. Mech. **25**, 169 (1981).
[59] V. R. Taylor and L. L. Stowe, Reflectance characteristics of uniform Earth and cloud surfaces derived from NIMBUS-7 ERB, J. Geogr. Res. **89**, 4987 (1984).
[60] L. Anselmo, P. Farinella, A. Milani, and A. M. Nobili, Effects of the Earth-reflected sunlight on the orbit of the LAGEOS satellite, Astron. Astrophys. **117**, 3 (1983), https://articles.adsabs.harvard.edu/pdf/1983A%26A...117...3A.
[61] D. P. Rubincam and N. S. Weiss, Earth Albedo and the orbit of LAGEOS, Celest. Mech. **38**, 233 (1986).
[62] F. Barlier, M. Carpino, P. Farinella, F. Mignard, A. Milani, and A. M. Nobili, Non-gravitational perturbations on the semimajor axis of LAGEOS, Ann. Geophys. **4**, 193 (1986).
[63] D. Lucchesi and P. Farinella, Optical properties of the Earth's surface and long-term perturbations of LAGEOS's semimajor axis, J. Geogr. Res. **97**, 7121 (1992).
[64] D. M. Lucchesi, Reassessment of the error modelling of non-gravitational perturbations on LAGEOS II and their impact in the Lense-Thirring determination. Part I, Planet. Space Sci. **49**, 447 (2001).
[65] U. Hugentobler, C. J. Rodriguez Solano, P. Steigenberger, R. Dach, and S. Lutz, Impact of Albedo modeling on GNSS satellite orbits and geodetic time series, in *Proceedings of the AGU Fall Meeting Abstracts* (AGU, San Francisco, 2009), Vol. 2009, pp. G11C–0654.
[66] C. J. Rodriguez-Solano, Impact of Albedo modelling on GPS orbits, Master Thesis, Ph.D. thesis, TUM, Munchen, 2009.
[67] B. A. Wielicki, B. R. Barkstrom, E. F. Harrison, Robert B. Lee III, G. L. Smith, and J. E. Cooper, Clouds and the Earth's radiant energy system (CERES): An Earth observing system experiment, Bull. Am. Meteorol. Soc. **77**, 853 (1996).
[68] D. P. Rubincam, Atmospheric drag as the cause of the secular decrease in the semimajor axis of LAGEOS's orbit, Geophys. Res. Lett. **7**, 468 (1980).
[69] J. Afonso, F. Barlier, C. Berger, and F. Mignard, The effect of atmospheric braking and electric drag on the trajectory of the LAGEOS satellite, Acad. Sci. Paris C. R. Ser. B **290**, 445 (1980).
[70] G. Afonso, F. Barlier, C. Berger, F. Mignard, and J. J. Walch, Reassessment of the charge and neutral drag of LAGEOS and its geophysical implications, J. Geophys. Res. **90**, 9381 (1985).
[71] C. Pardini, L. Anselmo, D. M. Lucchesi, and R. Peron, On the secular decay of the LARES semi-major axis, Acta Astronaut. **140**, 469 (2017).
[72] B. King-Hele, Theory of satellite orbits in an atmosphere, Q. J. R. Meteorol. Soc. **90**, 503 (1964).
[73] D. P. Rubincam, Drag on the LAGEOS satellite, J. Geophys. Res. **95**, 4881 (1990).
[74] D. Vokrouhlický and P. Farinella, Thermal force effects on slowly rotating, spherical artificial satellites—II. Earth infrared heating, Planet. Space Sci. **45**, 419 (1997).
[75] Y. Vigue, P. A. M. Abusali, and B. E. Schutz, Thermal force modeling for global positioning system using the finite element method, J. Spacecraft Rockets **31**, 855 (1994).
[76] H. F. Fliegel and T. E. Gallini, Solar force modeling of block IIR global positioning system satellites, J. Spacecraft Rockets **33**, 863 (1996).
[77] W. Marquis and C. Krier, Examination of the GPS block IIR solar pressure model, in *Proceedings of the 13th International Technical Meeting of the Satellite Division of the Institute of Navigation (ION GPS 2000), Salt Lake City, UT* (2000), pp. 407–415.
[78] J. Duha, G. B. Afonso, and L. D. D. Ferreira, Thermal re-emission effects on GPS satellites, J. Geodes. **80**, 665 (2006).
[79] The next generation of *Galileo* satellites will also be equipped with movable antennas for inter-satellite link.
[80] P. Steigenberger, S. Thoelert, and O. Montenbruck, GNSS satellite transmit power and its impact on orbit determination, J. Geodes. **92**, 609 (2018).
[81] Y. E. Bar-Sever, New and improved solar radiation pressure models for GPS satellites based on flight data, JPL-CA, Jet Propulsion Laboratory, California Institute of Technology Technical Report No. TR 80-4193, 1997.
[82] T. A. Springer, G. Beutler, and M. Rothacher, A new solar radiation pressure model for GPS, Adv. Space Res. **23**, 673 (1999).
[83] Y. Bar-Sever and D. Kuang, New empirically derived solar radiation pressure model for global positioning system satellites, Interplanet. Network Prog. Rep. **42–159**, 1 (2004), https://ipnpr.jpl.nasa.gov/progress_report/42-159/159I.pdf.
[84] Y. Bar-Sever and D. Kuang, New empirically derived solar radiation pressure model for global positioning system satellites during eclipse seasons, Interplanet. Network Prog. Rep. **42–160**, 1 (2005), https://ipnpr.jpl.nasa.gov/progress_report/42-160/160I.pdf.
[85] B. Fritsche, M. Ivanov, A. Kashkovsky *et al.*, Radiation pressure forces on complex spacecraft, HTG, Germany and ITAM, Russian, ESOC Contract 11908/96/D/IM, Technical Report TN, 1998.
[86] H. Klinkrad and B. Fritsche, Orbit and attitude perturbations due to aerodynamics and radiation pressure, ESTEC Technical Report TN, 1998.
[87] H. Klinkrad, C. Koeck, and P. Renard, Precise satellite skin-force modelling by means of Monte-Carlo ray tracing, ESA J. **14**, 409 (1990).
[88] H. Klinkrad, C. Koeck, and P. Renard, Key features of a satellite skin force modelling technique by means of Monte-Carlo ray tracing, Adv. Space Res. **11**, 147 (1991).
[89] M. Ziebart, High precision analytical solar radiation pressure modelling for GNSS spacecraft, Ph.D. Thesis, University of East London, 2001.
[90] M. Ziebart and P. Dare, Analytical solar radiation pressure modelling for GLONASS using a pixel array, J. Geodes. **75**, 587 (2001).
[91] B. Tan, Y. Yuan, B. Zhang, H. Z. Hsu, and J. Ou, A new analytical solar radiation pressure model for current BeiDou satellites: IGGBSPM, Sci. Rep. **6**, 32967 (2016).

[92] O. Montenbruck, P. Steigenberger, and F. Darugna, Semi-analytical solar radiation pressure modeling for QZS-1 orbit-normal and yaw-steering attitude, Adv. Space Res. **59**, 2088 (2017).
[93] Z. Li, Space vehicle radiation pressure modelling: A demonstration on Galileo satellites in GNSS, Ph.D. thesis, Department of Civil, Environmental and Geomagnetic Engineering, University of College London, 2018.
[94] Z. Li, M. Ziebart, S. Bhattarai, D. Harrison, and S. Grey, Fast solar radiation pressure modelling with ray tracing and multiple reflections, Adv. Space Res. **61**, 2352 (2018).
[95] G. Bury, R. Zajdel, and K. Sośnica, Accounting for perturbing forces acting on Galileo using a box-wing model, GPS Solut. **23**, 74 (2019).
[96] M. Ziebart, Analytical SRP model for GLONASS: Initial results, Applied Geodesy Research Unit, School of Surveying, University of East London Technical Report, 1998.
[97] M. Ziebart, Generalized analytical solar radiation pressure modeling algorithm for spacecraft of complex shape, J. Spacecraft Rockets **41**, 840 (2004).
[98] B. Rievers, C. Lämmerzahl, M. List, S. Bremer, and H. Dittus, New powerful thermal modelling for high-precision gravity missions with application to Pioneer 10/11, New J. Phys. **11**, 113032 (2009).
[99] F. Daraguna, Solar radiation pressure modeling for the QZS-1 satellite, Ph.D. thesis, Dipartimento di Ingegneria Industriale e Dipartimento di Fisica e Astronomia, Universitá degli Studi di Padova, Italy, 2017.
[100] F. Finke, Test of general relativity with GALILEO satellites, Ph.D. thesis, University of Bremen, 2023.
[101] P. Delva, N. Puchades, E. Schönemann, F. Dilssner, C. Courde, S. Bertone, F. Gonzalez, A. Hees, C. Le Poncin-Lafitte, F. Meynadier, R. Prieto-Cerdeira, B. Sohet, J. Ventura-Traveset, and P. Wolf, Gravitational redshift test using eccentric Galileo satellites: Supplemental material, Phys. Rev. Lett. **121**, 231101 (2018).
[102] F. Gini, GOCE precise non-gravitational force modeling for POD applications, Ph.D. thesis, CISAS, Padova, Italy, 2014.
[103] M. R. Drinkwater, R. Floberghagen, R. Haagmans, D. Muzi, and A. Popescu, VII: Closing session: GOCE: ESA's first Earth explorer core mission, Space Sci. Rev. **108**, 419 (2003).
[104] M. Meindl, G. Beutler, D. Thaller, R. Dach, and A. Jäggi, Geocenter coordinates estimated from GNSS data as viewed by perturbation theory, Adv. Space Res. **51**, 1047 (2013).
[105] K. Sośnica, G. Bury, R. Zajdel, D. Strugarek, M. Drożdżewski, and K. Kazmierski, Estimating global geodetic parameters using SLR observations to Galileo, GLONASS, BeiDou, GPS, and QZSS, Earth Planets Space **71**, 20 (2019).
[106] H. F. Fliegel, T. E. Gallini, and E. R. Swift, Global positioning system radiation force model for geodetic applications, J. Geophys. Res. **97**, 559 (1992).
[107] A. Jäggi, U. Hugentobler, and G. Beutler, Pseudo-stochastic orbit modeling techniques for low-Earth orbiters, J. Geodes. **80**, 47 (2006).
[108] G. Beutler, A. Jäggi, U. Hugentobler, and L. Mervart, Efficient satellite orbit modelling using pseudo-stochastic parameters, J. Geodes. **80**, 353 (2006).
[109] Galileo Metadata, https://www.gsc-europa.eu/support-to-developers/galileo-satellite-metadata#6.
[110] R. C. Willson, The total solar irradiance record and its continuity, in *Proceedings of AGU Fall Meeting Abstracts* (AGU, San Francisco, 2007), Vol. 2007, p. GC42A-03.
[111] Recall that the rotation of the Sun, since it varies with varying latitude, is of a differential type. The average rotation period is about 28-Earth days.
[112] G. de Toma, O. R. White, G. A. Chapman, and S. R. Walton, Solar irradiance variability: Progress in measurement and empirical analysis, Adv. Space Res. **34**, 237 (2004).
[113] S. K. Solanki and Y. C. Unruh, Solar irradiance variability, Astron. Nachr. **334**, 145 (2013).
[114] S. Lutz, M. Meindl, P. Steigenberger, G. Beutler, K. Sośnica, S. Schaer, R. Dach, D. Arnold, D. Thaller, and A. Jäggi, Impact of the arc length on GNSS analysis results, J. Geodes. **90**, 365 (2016).
[115] J. I. Andrés, R. Noomen, G. Bianco, D. G. Currie, and T. Otsubo, Spin axis behavior of the LAGEOS satellites, J. Geophys. Res. **109**, 2994 (2004).
[116] M. Visco and D. M. Lucchesi, Review and critical analysis of mass and moments of inertia of the LAGEOS and LAGEOS II satellites for the LARASE program, Adv. Space Res. **57**, 1928 (2016).
[117] M. Visco and D. M. Lucchesi, Comprehensive model for the spin evolution of the LAGEOS and LARES satellites, Phys. Rev. D **98**, 044034 (2018).
[118] M. Cheng, B. D. Tapley, and J. C. Ries, Deceleration in the Earth's oblateness, J. Geophys. Res. **118**, 740 (2013).
[119] B. D. Tapley and C. Reigber, The GRACE mission: Status and future plans, in *AGU Fall Meeting Abstracts* (AGU, San Francisco, 2001), p. G41C-02.
[120] G. Petit and B. Luzum, *IERS Conventions (2010)*, IERS Technical Note 36 (IERS, Verlag des Bundesamts für Kartographie und Geodäsie, Frankfurt am Main, 2010).
[121] D. M. Lucchesi, I. Ciufolini, J. I. Andrés, E. C. Pavlis, R. Peron, R. Noomen, and D. G. Currie, LAGEOS II perigee rate and eccentricity vector excitations residuals and the Yarkovsky-Schach effect, Planet. Space Sci. **52**, 699 (2004).
[122] Z. Li and M. Ziebart, Uncertainty analysis on direct solar radiation pressure modelling for GPS IIR and Galileo FOC satellites, Adv. Space Res. **66**, 963 (2020).
[123] F. Sapio *et al.*, following article, Fundamental physics measurements with Galileo FOC satellites and the Galileo for Science project. Part II: A box wing for modeling direct solar radiation pressure and preliminaries orbit determinations, Phys. Rev. D, **109**, 062005 (2024).
[124] This allows a better comparison with the intrinsic characteristics of an accelerometer to be used for the direct measurement of the main nongravitational accelerations. These direct measurements must be at least competitive with the indirect measurements provided by the models themselves. In fact, an advantage of an accelerometer compared to the models is provided by the process of integration of the measures, which translates into a more precise determination of the amplitude of the various disturbing effects.

[125] The L-band antenna is used for broadcasting the navigation message down to on ground receivers. SAR are UHF antennas designed to collect emergency messages from ships in evident danger and to be transmitted to search and rescue authorities. SAR antennas contribute to the international COSPAS-SARSAT system. The C-band antenna receives mission data and navigation corrections from uplink stations on the ground.
[126] www.sketchup.com.
[127] www.solidworks.com.
[128] Biovia, *Dassault systémes, solidworks, version 2017* (Dassault Systémes, San Diego, CA, 2017).
[129] COMSOL Multiphysics® Reference Manual, Version 5.5, COMSOL Multiphysics [Burlington, MA] (1998–2019).
[130] COMSOL Heat Transfer Module® User'S Guide, Version 5.4, COMSOL Multiphysics, [Burlington, MA] (1998–2018).
[131] https://www.mathworks.com.
[132] D. E. Pavlis *et al.*, *GEODYN II Operations Manual* (NASA GSFC, Greenbelt, 1998).
[133] D. M. Lucchesi and G. Balmino, The LAGEOS satellites orbital residuals determination and the Lense Thirring effect measurement, Planet. Space Sci. **54**, 581 (2006).